Seasonal dynamics and regional distribution patterns of CO_2 and CH_4 in the north-eastern Baltic Sea

Silvie Lainela[1], Erik Jacobs[2], Stella-Theresa Stoicescu[1], Gregor Rehder[2] and Urmas Lips[1]

[1]Department of Marine Systems, Tallinn University of Technology, Tallinn, 12618, Estonia
[2]Leibniz Institute for Baltic Sea Research Warnemünde, Rostock, 18119, Germany

Correspondence to: Silvie Lainela (silvie.lainela@taltech.ee)

Abstract. Significant research has been carried out in the last decade to describe the CO_2 system dynamics in the Baltic Sea. However, there is a lack of knowledge in this field in the NE Baltic Sea, which is the main focus of the present study. We analysed the physical forcing and hydrographic background in the study year (2018) and tried to elucidate the observed patterns of surface water CO_2 partial pressure (pCO_2) and methane concentrations (cCH_4). Surface water pCO_2 and cCH_4 were ~~calculated from~~ continuous~~ly~~ measure~~dments~~ during six monitoring cruises onboard R/V Salme, covering the Northern Baltic Proper (NBP), the Gulf of Finland (GoF) and the Gulf of Riga (GoR) and all seasons in 2018. The general seasonal pCO_2 pattern showed oversaturation in autumn-winter (average relative CO_2 saturation 1.2) and undersaturation in spring-summer (average relative CO_2 saturation 0.5) ~~in all three areas~~, but it locally reached the saturation level during the cruises in April, May and August in the GoR and in August in the GoF. cCH_4 was oversaturated during the entire study period, and the seasonal course was not well exposed on the background of high variability. Surface water pCO_2 and cCH_4 distributions showed larger spatial variability in the GoR and GoF than in the NBP for all six cruises. We linked the observed local maxima to river bulges, coastal upwelling events, fronts, and occasions when vertical mixing reached the seabed in shallow areas. Seasonal averaging over the CO_2 flux ~~based on our data~~ suggest~~s~~ a weak sink for atmospheric CO_2 for all basins, but high variability and the long periods between cruises (temporal gaps in observation) preclude a clear statement.

1 Introduction

Carbon dioxide (CO_2) and methane (CH_4) are important atmospheric greenhouse gases influencing the global climate. Changes in the levels of these trace gases are monitored in comparison with the pre-industrial era; however, precise and systematic atmospheric CO_2 and CH_4 measurements were not started before the late 1950s and early 1980s, respectively (Keeling et al., 2009; Dlugokencky et al., 1994). In the recent decade (2012-2021), the atmospheric CO_2 growth rate was 5.2 ± 0.02 GtC yr^{-1} (Friedlingstein et al., 2022). Atmospheric concentration of CH_4 remained nearly constant from the late 1990s through 2006, but resumed increasing since then, at an average rate of 7.6 ± 2.7 ppb yr^{-1} estimated for 2010–2019 (Canadell et al., 2023). Methane has large emissions from both natural (e.g. wetlands) and anthropogenic (e.g. enteric fermentation, manure treatment, fossil fuel exploitation) sources, but a clear demarcation of their nature is difficult (Canadell et al., 2023).

The global ocean is estimated to be a net sink of CO_2 (26 % of total CO_2 emissions during the decade 2012-2021; Friedlingstein et al., 2022). However, these global estimates are only beginning to resolve the net CO_2 source/sink characteristics of the coastal ocean. The complexity of processes in the coastal ocean and the limited data availability make it difficult to quantify regional carbon budgets and the coastal ocean's role in the global carbon budget. Although oceanic methane emissions play a modest role in the global methane budget (Reeburgh, 2007), estuaries and other coastal areas contribute up to 75% of all oceanic CH_4 emissions (Bange et al., 1994), with an important but not well quantified contribution of very shallow waters (Borges et al., 2016).

There is continuous gas exchange between the atmosphere and the marine environment. The exchange on the air-sea interface is controlled by the air-sea difference in gas concentrations (CO_2 or CH_4) and by the efficiency of the transfer processes. The solubility of gases in water and, thus, their air-sea exchange also depends on water temperature and salinity. The efficiency of air-sea exchange can be represented by the resistance of the surface and expressed in terms of a transfer velocity (Rutgersson et al., 2011), which is commonly parameterised as a function of wind speed (e.g. Wanninkhof 2014; Gutiérrez Loza et al., 2021).

In the Baltic Proper, the seasonal cycle of CO_2 is characterised by changing saturation levels between different seasons: oversaturation during autumn and winter and considerable undersaturation during spring and summer (Thomas and Schneider, 1999). Spring and summer periods are characterised by two distinct minima attributed to the spring phytoplankton bloom and the cyanobacteria bloom in midsummer, respectively (Schneider et al., 2014; Schneider and Müller, 2018). Understanding the surface water CO_2 dynamics in the Baltic Sea is becoming increasingly important since it is tightly linked to the biogeochemical processes, including primary production and nutrient (nitrogen and phosphorus) dynamics. In addition to the exchange at the air-sea interface and biological processes, the CO_2 system of surface waters in the Baltic Sea is influenced by the changes in hydrological and hydrographic conditions, e.g. river discharges, waves, currents, salinity and temperature, vertical stratification and mixing, upwelling/downwelling, fronts, etc. (e.g. Müller et al., 2016; Jacobs et al., 2021).

Methane is formed by microbial methanogenesis during the decomposition of organic material by microbial methanogenesis. CH_4 generated in the sediments that is not consumed at the sediment/water interface can diffuse into the water column and be transported over large areas of the Baltic Sea (e.g. Gülzow et al., 2014). CH_4 is consumed while approaching the surface water due to methane oxidation at the redoxcline and in the oxygenated water column above (Schmale et al., 2010; Jakobs et al., 2013 & 2014). This leads to strong vertical stratification with elevated concentrations in the sub-redoxcline layer and concentrations near atmospheric equilibrium at the sea surface (e.g. Schmale et al., 2010). Methanogenesis is generally more prevalent in shallower coastal regions due to the higher organic matter content (Valentine, 2002). In coastal areas, the dominant controlling factors for the seasonal variations of methane emission are the sediment organic matter content (Heyer and Berger,

2000), which might be modulated by seasonal deposition of fresh organic material from primary production, and temperature (Borges et al., 2018). In areas where the water column is relatively shallow and constantly mixed, CH_4 may escape into the atmosphere more readily. In general, the Baltic Sea is a source of atmospheric CH_4 (Bange et al., 1994; Gülzow et al., 2013), with the majority of methane emissions coming from shallow coastal areas (e.g. Roth et al., 2022). Outgassing can be intensified as a consequence of high water temperatures (Humborg et al., 2019) and processes driving vertical transport and mixing, e.g. upwelling events (Jacobs et al., 2021). Production in the upper, oxygenated water column might also contribute to or even govern methane sea-air fluxes (Schmale et al., 2018; Stawiarski et al., 2019), but it is of minor importance in the coastal ocean (Weber et al., 2019) and negligible in shallow coastal areas of high methane concentrations/emissions.

This work is the first extensive trace gas (CH_4 and CO_2) study in the north-eastern Baltic Sea area, with the main focus on the southern Gulf of Finland (GoF) and the Gulf of Riga (GoR), allowing the assessment of surface layer trace gas and carbon system dynamics in the region. The main aim of our work is to describe the spatial variability and seasonal dynamics of CO_2 and CH_4 and compare these patterns with the better studied Northern Baltic Proper (NBP) (Schneider et al., 2014; Schneider and Müller, 2018; Jakobs et al., 2014; Gülzow et al., 2013). We analysed the physical forcing and hydrographic and biological background in the study year (2018) and made an effort to link the observed patterns of CO_2 and CH_4 to these drivers.

The questions we try to answer are: Is the seasonal cycle of CO_2 and CH_4 in the southern GoF and GoR similar to that in the NBP? Can we elucidate regional differences in CO_2 and CH_4 dynamics due to river discharges, water depth and mixing, fronts and upwelling events, or other hydrographic features? Do the regional variations in CO_2 and CH_4 dynamics result in differences in yearly fluxes of these gases between the sub-basins? Our analysis is based on measurements during six reoccurring cruises of the Estonian monitoring programme in the north-eastern Baltic Sea (Fig. 1).

2 Study area

The Baltic Sea is a brackish, semi-enclosed sea in northern Europe. High freshwater runoff from the catchment area and sporadic saline water inflows from the North Sea maintain horizontal gradients and vertical stratification (e.g. Leppäranta and Myrberg, 2009). A quasi-permanent halocline exists at depths of 60-70 m in the deeper basins, and a seasonal thermocline develops at depths of 10-20 m from spring to autumn. The present study covers the following Baltic Sea sub-basins (Fig. 1): the NBP (we assign to it also a small fraction of the Eastern Gotland Basin), the GoF and the GoR.

The Northern Baltic Proper is the deepest sub-basin with a maximum depth of about 200 m and very variable topography and coastline. The quasi-permanent halocline separates oxygenated waters in the upper layers and hypoxic/anoxic waters below the halocline. However, no quasi-stationary horizontal gradients of environmental parameters exist in the surface layer. The general circulation pattern in the surface layer is considered mostly cyclonic (e.g. Placke et al., 2018). However, the presence

of the northward boundary current along the eastern coasts depends on local wind patterns and, as a consequence, downwelling and (less often) upwelling events and associated mesoscale currents may occur (Liblik et al., 2022).

The Gulf of Finland is an elongated basin (length about 400 km, width varies between 48 and 135 km) with a mean depth of 37 m (depths >100 m in the western gulf). Due to the direct connection to the NBP in the west and the largest freshwater discharge in the eastern end (Neva River), surface layer salinity decreases from about 6-7 g kg^{-1} at the entrance area to <2 g kg^{-1} in the easternmost area (e.g. Alenius et al., 1998). During winter, the water body is mixed fully in the shallower areas and down to the depth of the quasi-permanent halocline in deeper areas (Alenius et al., 2003). Hypoxic conditions are often observed below the halocline in the deeper areas (e.g. Stoicescu et al., 2019). General circulation in the surface layer is classically considered to be cyclonic (Andrejev et al., 2004), but could be seasonally variable (Maljutenko and Raudsepp, 2019). Energetic mesoscale features – eddies, fronts, upwelling events, etc. (Pavelson, 2005; Lips et al., 2016a; Kikas and Lips, 2016) may frequently occur. The largest freshwater source along the research vessel (R/V) track analysed in the present study is the Narva River in the south-eastern GoF. Depending on the seasonally varying runoff and local wind conditions, the river water spreads towards the open sea or along the coast and mixes with the gulf water masses (Laanearu and Lips, 2003).

The Gulf of Riga is a semi-enclosed shallow basin with a mean depth of 26 m (Ojaveer, 1995) and a maximum depth of the central basin of 56 m (Stiebrins and Väling, 1996). Freshwater discharge originates mostly from five larger rivers (Daugava, Lielupe, Gauja, Pärnu, and Salaca) in the southern and eastern parts of the gulf (Yurkovskis et al., 1993). Saltier waters from the Baltic Proper enter the gulf via the Irbe Strait in the west (about 70-80% of water exchange) and the Suur Strait in the north (Astok et al., 1999). The whole-basin circulation in the surface layer depends on the prevailing wind pattern – it is mostly cyclonic, but anti-cyclonic in summer (Lips et al., 2016b). Anti-cyclonic circulation could also prevail in the southern gulf, connected to the discharges from the Daugava and Lielupe rivers (Soosaar et al., 2016). Due to the shallowness of the basin, the water column is fully mixed in autumn-winter. Thermal stratification starts to develop in April and decays in October-December, depending on the water depth and yearly variable meteorological conditions (Skudra and Lips, 2017; Stoicescu et al., 2022). Near-bottom seasonal hypoxia can be observed in the deeper areas of the central gulf (Stoicescu et al., 2022).

The research vessel track reached the southern gulf close to the largest river discharges (Daugava and Lielupe) and the Pärnu Bay, which is shallow and under the influence of the Pärnu River discharge. The measurements were also conducted in the Väinameri Sea – the shallow and sheltered sea area (average depth of 5-10 m) between the mainland and the western Estonian islands.
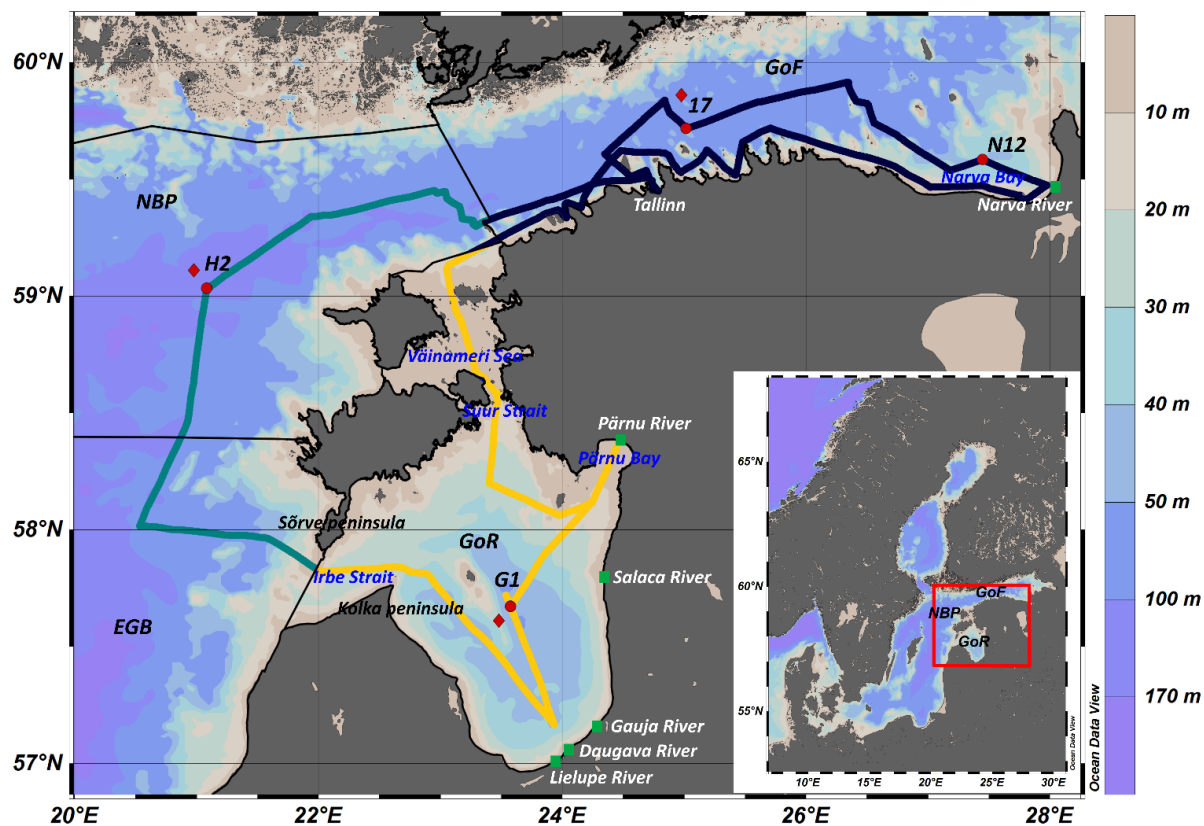
Figure 1: Map of the study area with bottom topography: GoF – Gulf of Finland (blue cruise track), NBP – Northern Baltic Proper (green) and GoR – Gulf of Riga (yellow) (according to HELCOM sub-basins division, marked with black lines). Green-filled squares denote river runoffs. Red-filled circles represent the locations of the most characteristic stations of the sub-basins. Red-filled diamonds denote the closest meteorological ERA5 data grid points to the sub-basins' most characteristic stations. This map was generated using Ocean Data View 5.6.3 software (Schlitzer, 2022).

3 Material and methods

The spatial variability and seasonal dynamics of CO_2 and CH_4 in three sub-basins of the north-eastern Baltic Sea in the study year are characterised. The results are analysed considering the background meteorological and hydrographic conditions, e.g., upper mixed layer (UML) temperature and depth, bottom depth vs UML depth, fronts and upwelling events, and seasonal and spatial patterns of Chl *a* distribution in the surface layer. Also, CO_2 and CH_4 fluxes are estimated for all studied areas. Measurement approaches, additional data sources and calculation methods are described below.

3.1 Meteorological information

Meteorological conditions were evaluated by ERA5 comprehensive reanalysis data (from Copernicus Climate Data Store; Hersbach et al., 2019). Surface net solar radiation, air temperature at 2 m above the sea surface and winds at 10 m above the sea surface were extracted for the positions closest to the monitoring stations 17, G1 and H2 in the GoF, GoR and NBP,

respectively (see Fig. 1). For the comparison of the study year (2018) and the long-term (1979-2018) meteorological
145 conditions, ERA5 data at station NBP were used. Monthly average reanalysis values in 2018 are presented against the long-term monthly averages and variability, characterised by standard deviations and minimum and maximum values. Average wind vectors and wind roses were calculated for the selected stations in the GoF, GoR and NBP (Fig. 1) for the cruise periods using 2018 hourly reanalysis data. The presented wind characteristics during the cruises represent seven-day periods ending at the cruise termination date, i.e. periods containing 1-2 days before the cruise up to its end.

150 **3.2 Continuous surface water measurements aboard R/V Salme**

The measurements were conducted using a flow-through system (Ferrybox) onboard R/V Salme during six monitoring cruises in 2018: on 8-12 January, 16-20 April, 28 May-2 June, 9-13 July, 22-27 August, and 22-28 October. The Ferrybox by Go-systemelektronik was equipped with an SBE38 sensor for temperature, an SBE45 MicroTSG sensor for temperature and conductivity, WetLabs *ECO* FL and Turner Design Cyclops-7 sensors for chlorophyll *a* fluorescence and a digital optode by
155 PONSEL for dissolved oxygen measurements. The Ferrybox water intake was located at a depth of 2 m. The sampling interval was 1 minute, corresponding to a nominal spatial resolution of about 250 m while the vessel was moving with its normal cruising speed of 8-9 knots.

The Ferrybox was supplemented with the equipment for trace gas (CO_2 and CH_4) measurements using an equilibrator setup.
160 During the first cruise in January, a LI-COR 6262 CO_2/H_2O instrument coupled to the headspace of a glass equilibrator (similar to Gülzow et al., 2011) was used. During the other cruises, the setup was similar to the MESS presented in Sabbaghzadeh et al. (2021) using a Los Gatos Research CH_4/CO_2 analyser, but with a lower water flow of around 2.5–4.5 L min^{-1}. In July and October, the e-folding response times of the setup were exemplarily determined to be 720 s and 790 s for CH_4 and 35 s and 52 s for CO_2; the lower values in July illustrate the influence of higher water temperature (ca. 18 vs. 12.5 °C) and higher water
165 flow (ca. 3.6 vs. 3.1 L min^{-1}). Apart from January, an additional Microx 4 oxygen meter PSt7 optode measured dissolved oxygen in the water supply line of the equilibrator.

Atmospheric pressure was measured during the entire cruise, and measurements of atmospheric CO_2 and CH_4 (as mole fractions in ppm/ppb) were performed 1-2 times per cruise. For this, the gas supply of the trace gas analyser was switched
170 from the equilibrator to a long tubing used to sample air on the windward side of the upper deck.

The data series contain surface layer temperature, salinity, chlorophyll *a* concentration (Chl *a*), partial pressure of CO_2 (pCO_2), dissolved oxygen concentration and concentration of CH_4 (cCH_4) with a spatial resolution of about 250 m along the cruise tracks with a length of about 1500 km each, covering three Baltic Sea sub-basins.

3.3 Quality assurance and processing of continuous flow-through data

A two-step calibration procedure was followed for the Ferrybox Chl a fluorescence data. First, a linear regression was found between Chl a fluorescence data from the CTD (Ocean Seven 320$plus$, Idronaut s.r.l., with Seapoint fluorometer) and Chl a concentrations determined in the laboratory from the water samples collected at respective stations and depths. Chl a concentration in the laboratory was determined optically by spectrophotometry (HELCOM, 2017). Afterwards, a linear regression between the calibrated Chl a data from CTD at 2 m depth and Ferrybox Chl a fluorescence data was found. This calibration procedure was performed separately for each cruise.

The same two-step calibration procedure was used for dissolved oxygen measurements during the cruises in January and April. Dissolved oxygen concentrations from water samples were determined electrochemically using a dissolved oxygen meter (OX 400 1 DO analyzer; WWR International, LCC), also taking into account a salinity correction. For other cruises, the Microx 4 oxygen meter PSt7 optode data was used. Oxygen partial pressures (pO_2) from the PSt7 optode were post-calibrated using discrete sample measurements conducted at 1 m depth at monitoring stations. The procedure was followed separately for each cruise, assuming that the first and last discrete measurements were representative for the start and end of each cruise.

Measured CO_2 and CH_4 mole fractions (xCO_2/xCH_4) were post-calibrated using a near-atmospheric standard gas (398.49 ppm CO_2, 1.91 ppm CH_4, matrix: ambient air). These target measurements were performed at the beginning and end of each cruise and almost every day at sea to achieve a drift correction if necessary. Measured xCO_2 and xCH_4 were converted into dry-air values based on water mole fractions measured by the same instrument. From these, the partial pressures (pCO_2/pCH_4) were calculated assuming 100 % humidity in the equilibrator headspace (water vapour pressure by Weiss and Price, 1980). pCO_2 was temperature-corrected to account for water warming from the inlet to the equilibrator (Takahashi et al., 1993). CH_4 partial pressure data were converted to concentration (cCH_4) using the solubility constants given in Wiesenburg and Guinasso (1979). All equilibrator data were averaged using a 1-minute rolling mean to match the temporal resolution of other Ferrybox parameters.

Despite the fact that we actually recorded mole fractions (xCO_2 and xCH_4), we report our CO_2 data as pCO_2 and CH_4 data as cCH_4, considering that these units are usually reported in studies addressing the respective gases. Accordingly, the atmospheric data were displayed as atmospheric partial pressure for CO_2 or saturation concentration calculated from temperature and salinity for CH_4.

Surface flow-through pCO_2 and cCH_4 data recorded at the monitoring stations were excluded, using a speed of the vessel of less than 0.6 knots as criterion. This was necessary because during profiling and water sampling, the sampling device or ship propulsion could bring up sub-surface water, which caused artificial spikes in pCO_2 and cCH_4 signals.

3.4 CTD profiles and upper mixed layer depth

Vertical profiles of temperature, salinity, Chl a fluorescence and dissolved oxygen were recorded at the monitoring stations
210 using the CTD probe (Ocean Seven 320plus; Idronaut s.r.l). Salinity and density anomaly are shown as absolute salinity (g kg^{-1}) and sigma-0 (kg m^{-3}), respectively, and were calculated using the TEOS-10 equation of state (IOC et al., 2010). The depth of the UML was determined from the CTD profiles at the monitoring stations ~~for all six monitoring cruises~~to evaluate whether vertical mixing reached all the way down to the seabed. It was done by comparing the UML depth with the water depth along the ship track adjacent to each station. The UML depth was defined according to Liblik and Lips (2012) as the minimum depth,
215 where $\rho_z - \rho_3 > 0.25$ kg m^{-3}, where ρ_z is the density anomaly at depth z and ρ_3 at depth 3 meters.

3.5 Air-sea CO_2 and CH_4 flux calculations

Air-sea gas exchange calculations were performed using the FluxEngine toolbox. The FluxEngine toolbox is an open-source software package described in more detail by Shutler et al. (2016) and Holding et al. (2019).

220 The CO_2 fluxes were calculated using a rapid model approach (Woolf et al., 2016) implemented into the FluxEngine toolbox:

$$F = k(\alpha_W pCO_{2_W} - \alpha_A pCO_{2_A}), \tag{1}$$

where F (g C m^{-2} day^{-1}) denotes the flux across the interface, k the gas transfer velocity, α the solubility of gas in the subsurface water and the water surface ~~seawater/air-sea interface~~ (subscripts W and A, accordingly) and pCO_2 partial pressure of CO_2 in the sea surface water/atmosphere (subscripts W and A, accordingly).

225

Methane fluxes were calculated using the same approach as for CO_2 fluxes:

$$F = k(~~\alpha_W~~ cCH_{4_W} - ~~\alpha_A~~ cCH_{4_A}), \tag{2}$$

where cCH_4 is concentration of CH_4 in the surface sea water/atmosphere (subscripts W and A, accordingly).

230 In order to accurately describe the fluxes and the carbon budget, it is essential to include relevant processes to the air–sea CO_2 and CH_4 flux parametrisation. Nightingale et al. (2000) was used for the gas transfer velocity parametrisation for both CO_2 and CH_4 in our study. The sensitivity analysis of the gas transfer velocity in the Baltic Sea (Gutiérrez-Loza et al., 2021) used different parametrisations of the gas transfer velocity to evaluate the effect of other relevant processes in addition to wind speed on the net CO_2 flux at regional and sub-regional scale. In the Estonian sea area, they observed negligible differences in
235 the average net CO_2 flux ~~were observed~~ when using the different gas transfer parametrisations relative to the wind-based parametrisation ~~(Nightingale et al. 2000). Therefore Nightingale et al. (2000) was used for the gas transfer velocity parametrisation for both CO₂ and CH₄ in our study~~:

$$k = (0.222U_{10}^2 + 0.333U_{10})\sqrt{600/Sc}, \tag{3}$$

where U_{10} is the wind speed at 10 m above the sea surface and Sc is the Schmidt number. The Schmidt number parametrisation was based on Wanninkhof (2014).

4 Results

4.1 Meteorological conditions

Meteorological conditions in the Baltic Sea area in 2018 were characterised by warmer than long-term average air and sea surface temperatures (Hoy et al., 2020; Humborg et al., 2019). Net solar radiation was above the average seasonal curve from February to September, with the maximum positive deviation in May (Fig. 2). In accordance with the latter, the monthly mean air temperature exceeded the long-term average from April until the end of the year. Except for June, the monthly mean wind speed in the spring and summer of 2018 was lower than the long-term average. All these meteorological parameters predict that the sea surface temperature should have been higher and seasonal vertical stratification stronger than on average due to the increased positive buoyancy flux and weak wind-induced mixing.

The winds from west and south-west prevailed during and before the cruises in January, April and August (Fig. 2), which is in accordance with the general airflow in the study area. During the cruises in July and October, the wind direction was generally from north or north-east, while weak winds from the same direction prevailed in May-June. Note that the northerly and north-easterly winds in July and October were favourable for the upwelling development along the southwestern coast of the Gulf of Finland and the eastern coasts in the Northern Baltic Proper.

The variability in wind speed and direction between the three basins and within the cruise periods is presented by the wind roses (see Fig. 3, where wind roses for three cruise periods with larger wind forcing and spatial variability are presented). The winds were mostly from one direction during the cruise in August, and a wider spread was characteristic for the cruise periods in July and October. In July, mostly two directions prevailed – easterly winds, which could cause upwelling events along the entire southern coast of the Gulf of Finland, and north-westerly winds, which are upwelling favourable for the eastern coasts of the NBP. In October, the spread of directions was the largest, but the strongest winds with speeds exceeding 15 m s^{-1} in the GoF and NBP were from the north-east. In the GoR, wind speeds were generally lower than in the other two basins.
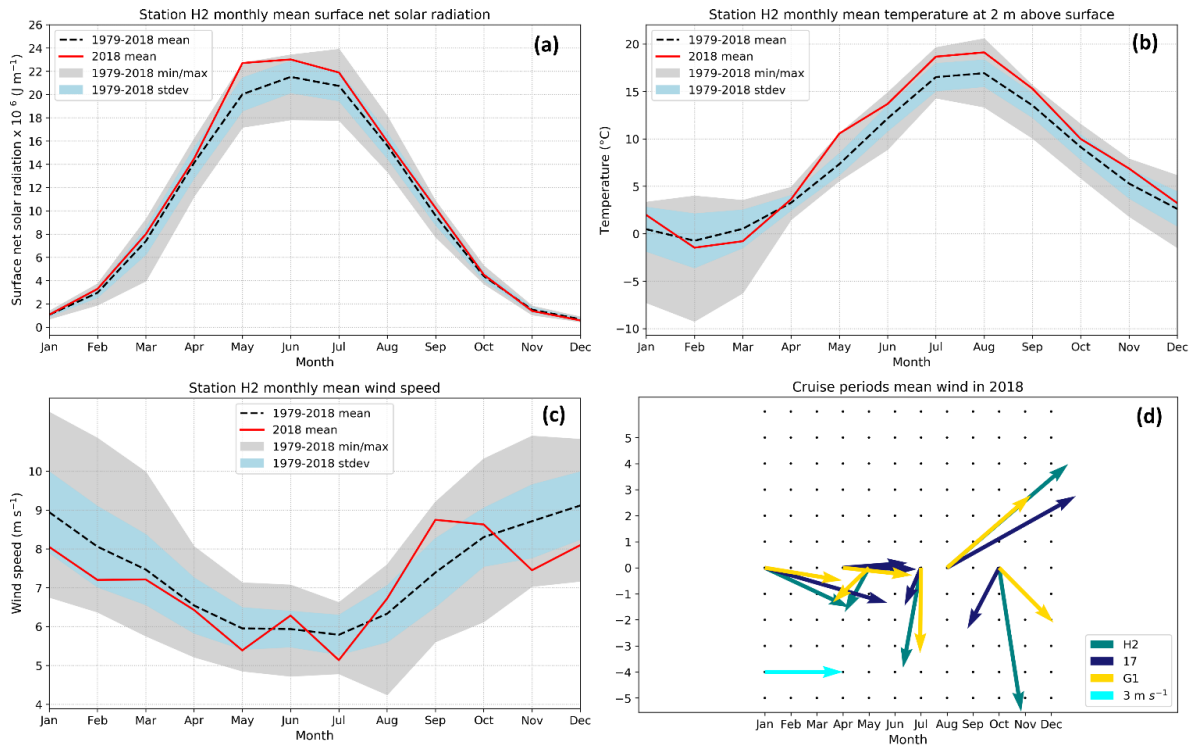
Figure 2: Monthly average (a) surface net solar radiation, (b) air temperature and (c) wind speed in 2018 (red line) compared with the long-term averages (dashed black line), standard deviations (blue area) and minimum-maximum values (grey area) in the NBP (station H2) for the period 1979-2018. (d) Cruise-period average wind vectors in the NBP (H2, green), GoF (17, blue) and GoR (G1, yellow). See the locations of stations and model grid points for data extraction in Fig. 1.
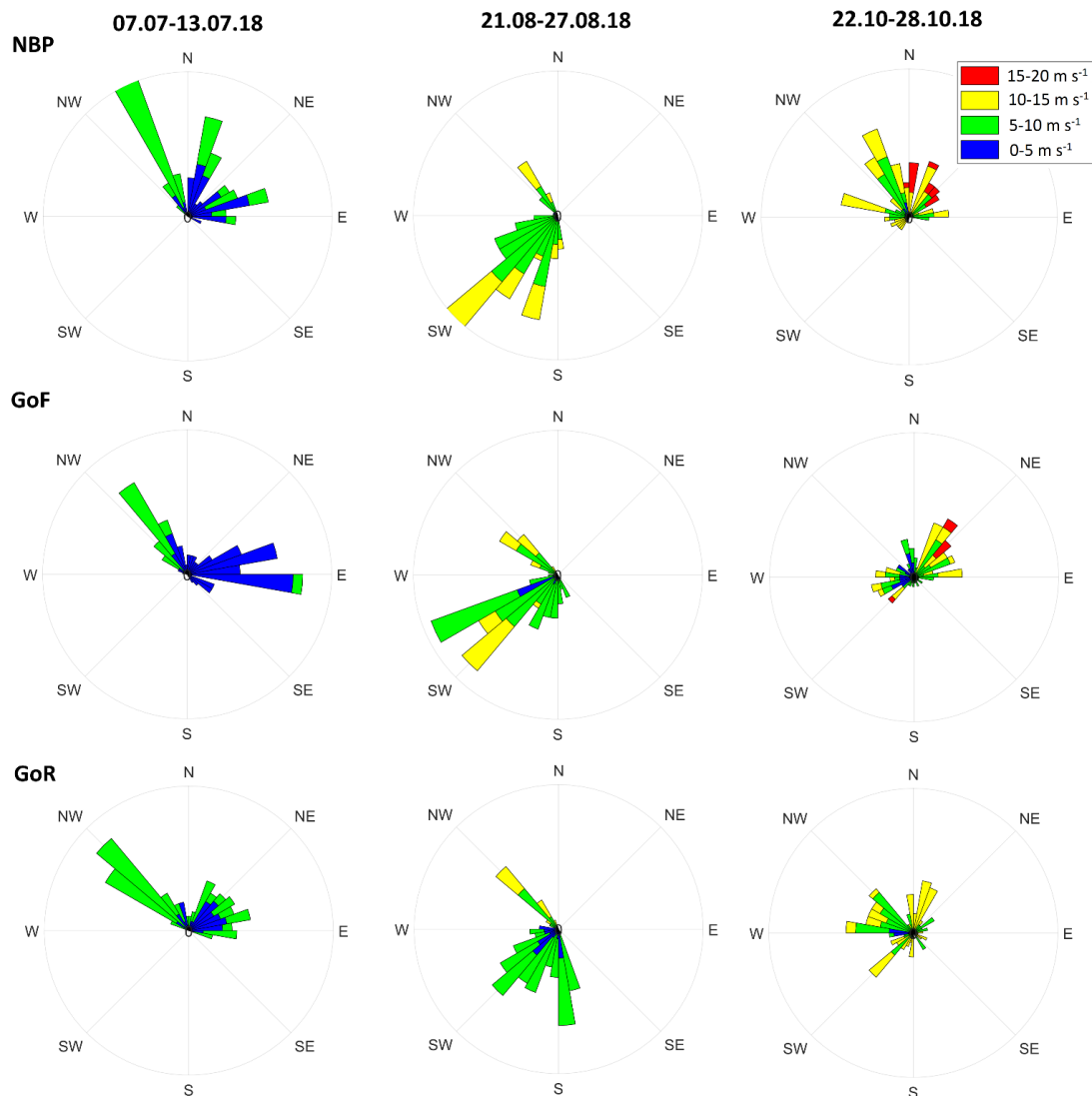
Figure 3: Cruise-period wind roses in May-June (left column), July (middle column) and August (right column) 2018 in the NBP (upper row), GoF (middle row) and GoR (lower row) based on the hourly ERA5 data extracted from a grid point close to the monitoring stations H2, 17 and G1, respectively (see locations in Fig. 1). Radial axis maximum is 30 (out of 168).

275 **4.2 Spatial variability**

Surface water pCO_2 and cCH_4 distributions along the R/V track show larger spatial variability in the GoR and GoF than in the NBP for all six cruises (Figs. 4-9). Although the general seasonal pCO_2 course ~~with CO₂ oversaturation in the surface layer in winter and autumn and undersaturation in spring–summer~~ is evident, pCO_2 locally exceeded the atmospheric equilibrium level also during the cruises in April, May and August. The latter is mostly valid for the GoR but also for the GoF in August. cCH_4

280 was oversaturated in the surface layer during the whole study period, with prominent local peaks of cCH_4 in the GoR and GoF.

In January (Fig. 4), surface water pCO_2 along the cruise track (Fig. 4c) did not show remarkable regional differences. Values fluctuated within the range of 425 – 550 µatm and were oversaturated in all monitored areas. Almost in all areas, the water column was well-mixed down to the seabed or permanent halocline. Note that in contrast to the other cruises, the vessel did

285   not visit mouth areas of the rivers (neither in the GoR nor in the GoF) and cCH_4 was not measured in January.

The cruise in April (Fig. 5) mapped pCO_2 and cCH_4 distributions in the period of the onset of seasonal stratification and spring bloom in different development phases. The surface water pCO_2 (Fig. 5c) was mostly below the atmospheric partial pressure but reached equilibrium with the atmosphere in the western and central GoR. Low Chl a and oxygen concentrations indicate

290   that the spring bloom was yet in its initial phase in this area (Fig. 5d). Also, the water column was mixed almost down to the seabed in this sea area. The pCO_2 values were clearly lower in the eastern part of the open GoR and the shallow Pärnu Bay and the Väinameri Sea. These pCO_2 minima (down to 60 µatm) were associated with increased temperature and the highest Chl a and oxygen concentrations in these areas, while the influence of the Pärnu River was visible via a local peak in the pCO_2 (up to 397 µatm).

295

From the western GoF towards the central GoF, a Chl a increase from <9 to 15 mg m^{-3} was accompanied by slightly higher oxygen and lower pCO_2 values (about 130 µatm). ~~Interestingly,~~Although high Chl a concentrations up to 16 mg m^{-3} were mapped along the south-eastern coast of the GoF, ~~but~~ pCO_2 values in this area remained on a higher level~~,~~ (around 250 µatm)~~,~~ than in other regions with a similar surface layer Chl a content. Note that the water column along the coast, except close to the

300   Narva River mouth, was well mixed down to the seabed. Elevated cCH_4 ~~were~~was measured, similar to the pCO_2 distribution, in the western and central GoR (27-37 nmol L^{-1}) and in the Pärnu Bay close to the mouth of the Pärnu River (40 nmol L^{-1}). ~~The high methane concentration in the central GoR could be related to the absence of vertical stratification and the almost fully mixed water column.~~ Elevated cCH_4 ~~were~~was also measured along the south-western coast of GoF (26 nmol L^{-1}; marked as SW GoF in Fig. 5e), where the water column was mixed down to the seabed, and close to the mouth of the Narva River (up

305   to 30 nmol L^{-1}). The direct influence of the Pärnu River and Narva River was expressed by the cCH_4 peaks.

The cruise at the end of May and beginning of June (Fig. 6) coincided with the phytoplankton summer minimum, while the water column was characterised by unusually high sea surface temperatures (13-18 °C; Fig. 6b) and shallow upper mixed layer (Fig 6a, on average <6 m in the GoR and 8 m in the central GoF). The pCO_2 values had decreased to the minimum along most

310   of the ship track, varying mostly between 50 and 100 µatm, while moderately higher (reaching 200 µatm) than background pCO_2 values were registered ~~occasionally in the NBP accompanied by locally lower temperatures at 2 m depth and~~ in the NBP-GoR transition area, the Irbe Strait. CO_2 oversaturation was locally recorded in the GoR shallowest areas – the Pärnu Bay and the Väinameri Sea. In the Narva Bay, no distinct Narva River impact was registered. Local cCH_4 maxima were observed in the shallow bays of the southern and south-western GoF (>80 nmol L^{-1}) and in the Irbe Strait, close to the Kolka peninsula

(>35 nmol L^{-1}). Only slightly higher than background cCH$_4$ values were measured in the southern GoR close to the mouths of the largest rivers – Daugava and Lielupe. ~~As indicated by the salinity distribution, the vessel almost did not pass the waters with strong river influence.~~ In contrast, an extensive peak in cCH$_4$ was registered in the shallow Pärnu Bay close to the Pärnu River (maximum measured concentration was 232 nmol L^{-1}). Local maxima in the shallow Väinameri Sea increased to notable peaks along the south-western coast of GoF. Local maxima of 33 nmol L^{-1} in the Narva Bay were likely due to the Narva River influence.

In mid-July (Fig. 7), the surface waters were undersaturated in CO$_2$ along the entire ship track (Fig. 7c; note that the vessel did not visit the mouth areas of the Pärnu and Narva rivers). The UML has slightly deepened in the GoR (8 m), but was the shallowest in the offshore GoF (<7 m). Higher than 5 mg m^{-3} Chl a concentrations were observed in the offshore areas of NBP, north-eastern GoR and central GoF, probably due to the development of the summer bloom. Elevated pCO$_2$ values were recorded in parts of the NBP offshore areas (330 µatm) and the coastal sea area, in the Irbe Strait (310 µatm) and the Väinameri Sea (355 µatm). Local maxima of cCH$_4$ up to 43 nmol L^{-1} were observed in the shallow bays of the southern and south-western GoF, including the transition area into the GoF. In comparison with the cruise at the end of May, in July, a relatively low cCH$_4$ peak (14 nmol L^{-1}) was observed in the Irbe Strait, and the influence of large rivers in the southern GoR was almost not detectable.

In August (Fig. 8), CO$_2$ varied around the saturation level. The surface waters were undersaturated in CO$_2$ ~~was undersaturated~~ in most areas of the GoF except the Narva Bay, where the water column was well-mixed down to the seabed, oversaturated in the Väinameri Sea and Pärnu Bay, and undersaturated in the NBP (Fig. 8c). These higher pCO$_2$ values were characteristic for the shallow areas and could be only partly related to the river discharge (as in the Narva Bay and the Pärnu Bay). A distinct local maximum in pCO$_2$ of 460 µatm was related to the salinity front in the Irbe Strait, as also observed earlier. Local cCH$_4$ maxima were observed in the shallow bays of the southern and south-western GoF and along the south-eastern coast in the Narva Bay. Locally, well-pronounced cCH$_4$ peaks with a maximum concentration of 177 nmol L^{-1} were also observed in the Väinameri Sea and Pärnu Bay ~~(probably influenced by the Pärnu River discharge)~~. The increase in cCH$_4$ in the Irbe Strait (38 nmol L^{-1}) was comparable with the cCH$_4$ peak at the end of May cruise.

In October (Fig. 9), surface waters were oversaturated in CO$_2$ almost along the entire ship track (Fig. 9c). Like during the August cruise, pCO$_2$ values were lower in the NBP (varying between 400 and 480 µatm) than in the GoF and GoR (varying up to 600 µatm). In contrast to the summer cruises, higher pCO$_2$ values were characteristic for the offshore areas in the GoR, and lower values were present in the shallow coastal sea areas – the Pärnu Bay and the Väinameri Sea. pCO$_2$ values ~~slightly~~ exceeding 1200 µatm were registered in connection to an upwelling event in the SW GoF caused by the strong north-westerly winds before and during the cruise. ~~This upwelling event was caused by the strong north-westerly winds before and during the cruise (Figs. 2 and 3) and is better seen in salinity than temperature distribution (Fig. 9b).~~ Peaks in cCH$_4$ up to 80 nmol L^{-1}

were registered in the shallow bays along the southern coast of GoF ~~and also in the shallow coastal area in the NBP (off~~

350   ~~Saaremaa Island) that was not visited during the earlier cruises~~. In the Irbe Strait, cCH$_4$ increased up to 15 nmol L^{-1} in October.

A clear cCH$_4$ peak of 62 nmol L^{-1} was detected in the Pärnu Bay, probably influenced by the Pärnu River discharge. Local

maxima in the Väinameri Sea increased to an extensive broad peak (69 nmol L^{-1}) in the upwelling waters in the SW GoF.

Cruise in January
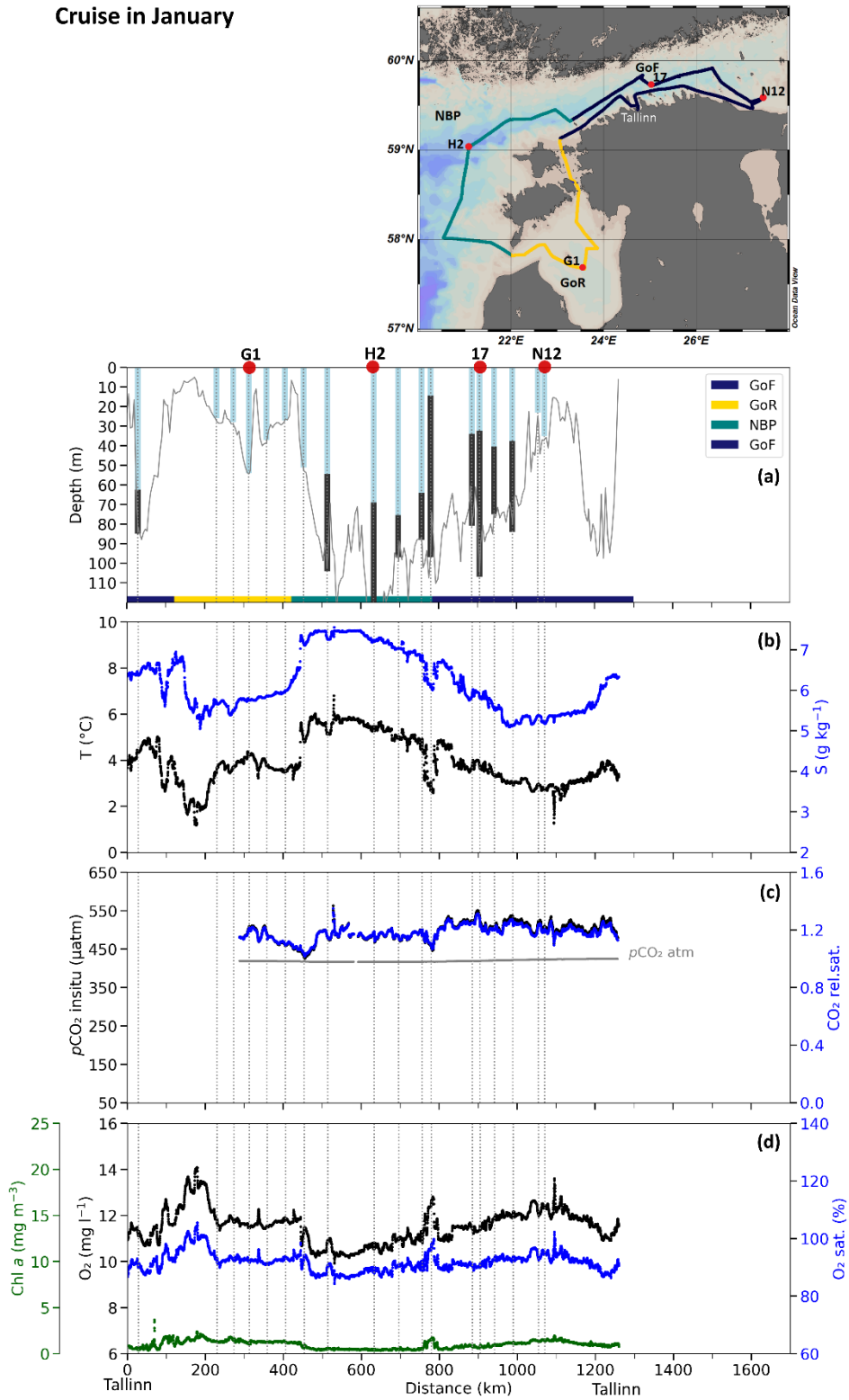
Figure 4: January monitoring cruise (8-12 January): The trajectory is shown on the map and on panel (a) UML depth (light blue bars) and the water column extent below the UML (dark blue bars); vertical grey dashed lines indicate the locations of monitoring stations, the locations of the most characteristic stations of the sub-basins are denoted with red dots. (b) Spatial variability of temperature (left y-axis) and salinity (right y-axis), (c) CO_2 partial pressure (left y-axis) and relative saturation (right y-axis), and (d) Chl a (left y-axis), dissolved oxygen concentration (left y-axis) and saturation (right y-axis). The x-axis denotes the distance (in km) from the start of the monitoring cruise (Tallinn).

Cruise in April
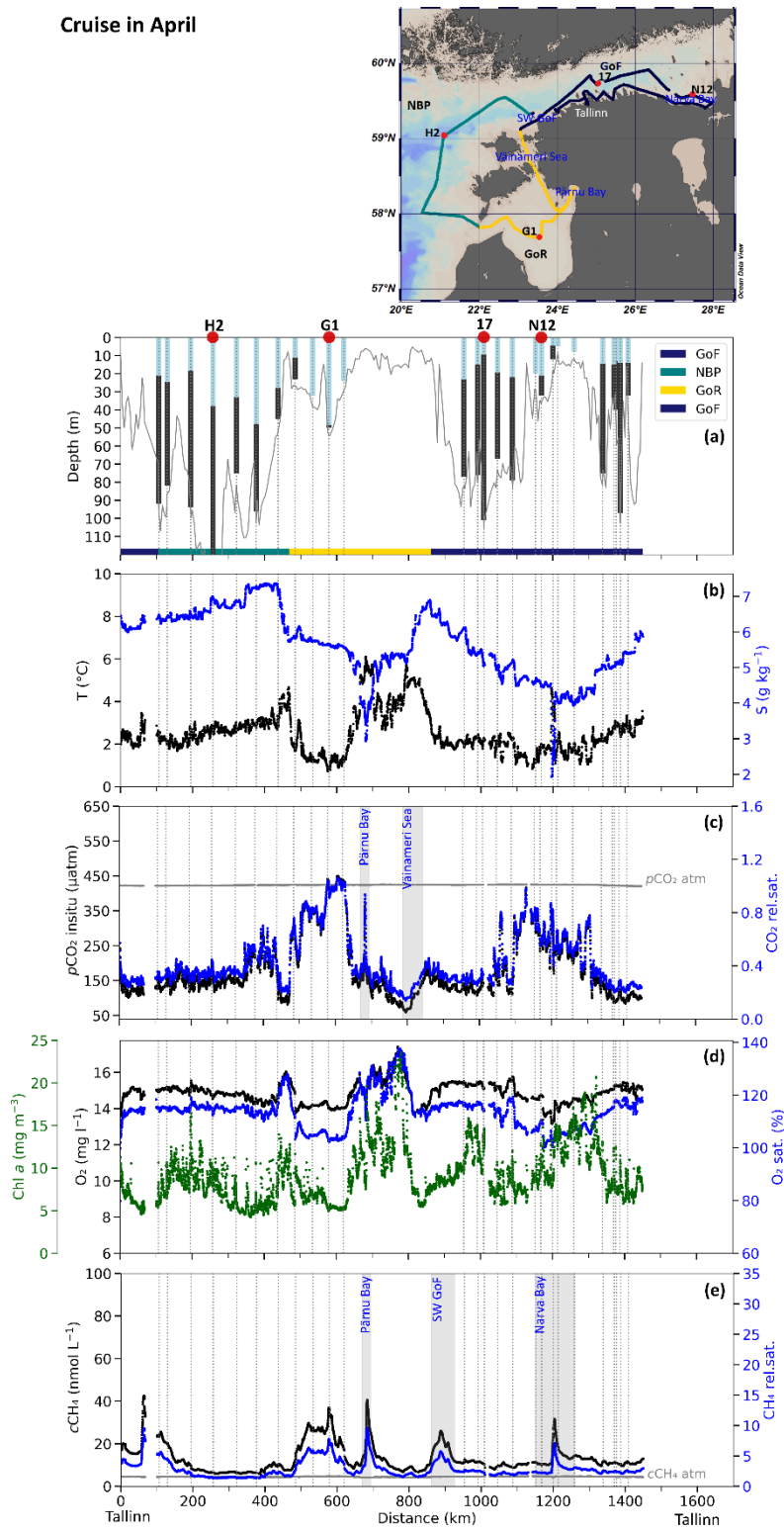
Figure 5: April monitoring cruise (16-20 April): The trajectory is shown on the map and on panel (a) UML depth (light blue bars) and the water column extent below the UML (dark blue bars); vertical grey dashed lines indicate the locations of monitoring stations, the locations of the most characteristic stations of the sub-basins are denoted with red dots. (b) Spatial variability of temperature (left y-axis) and salinity (right y-axis), (c) CO_2 partial pressure (left y-axis) and relative saturation (right y-axis), (d) Chl *a* (left y-axis), dissolved oxygen concentration (left y-axis) and saturation (right y-axis), and (e) CH_4 concentration (left y-axis) and relative saturation (right y-axis). The x-axis denotes the distance (in km) from the start of the monitoring cruise (Tallinn).

365

Cruise at the end of May

Figure 6: End of May monitoring cruise (28 May-2 June): The trajectory is shown on the map and on panel (a) UML depth (light blue bars) and the water column extent below the UML (dark blue bars); vertical grey dashed lines indicate the locations of monitoring stations, the locations of the most characteristic stations of the sub-basins are denoted with red dots. (b) Spatial variability of temperature (left y-axis) and salinity (right y-axis), (c) CO_2 partial pressure (left y-axis) and relative saturation (right y-axis), (d) Chl *a* (left y-axis), dissolved oxygen concentration (left y-axis) and saturation (right y-axis), and (e) CH_4 concentration (left y-axis) and relative saturation (right y-axis). The x-axis denotes the distance (in km) from the start of the monitoring cruise (Tallinn). In May, cCH_4 signal in the river estuaries was extreme in comparison with the rest of the data, and this signal was cut on the panel to 100 nmol L^{-1} to properly display the structure within low-concentration areas. Note different scale for temperature in comparison with January and April.
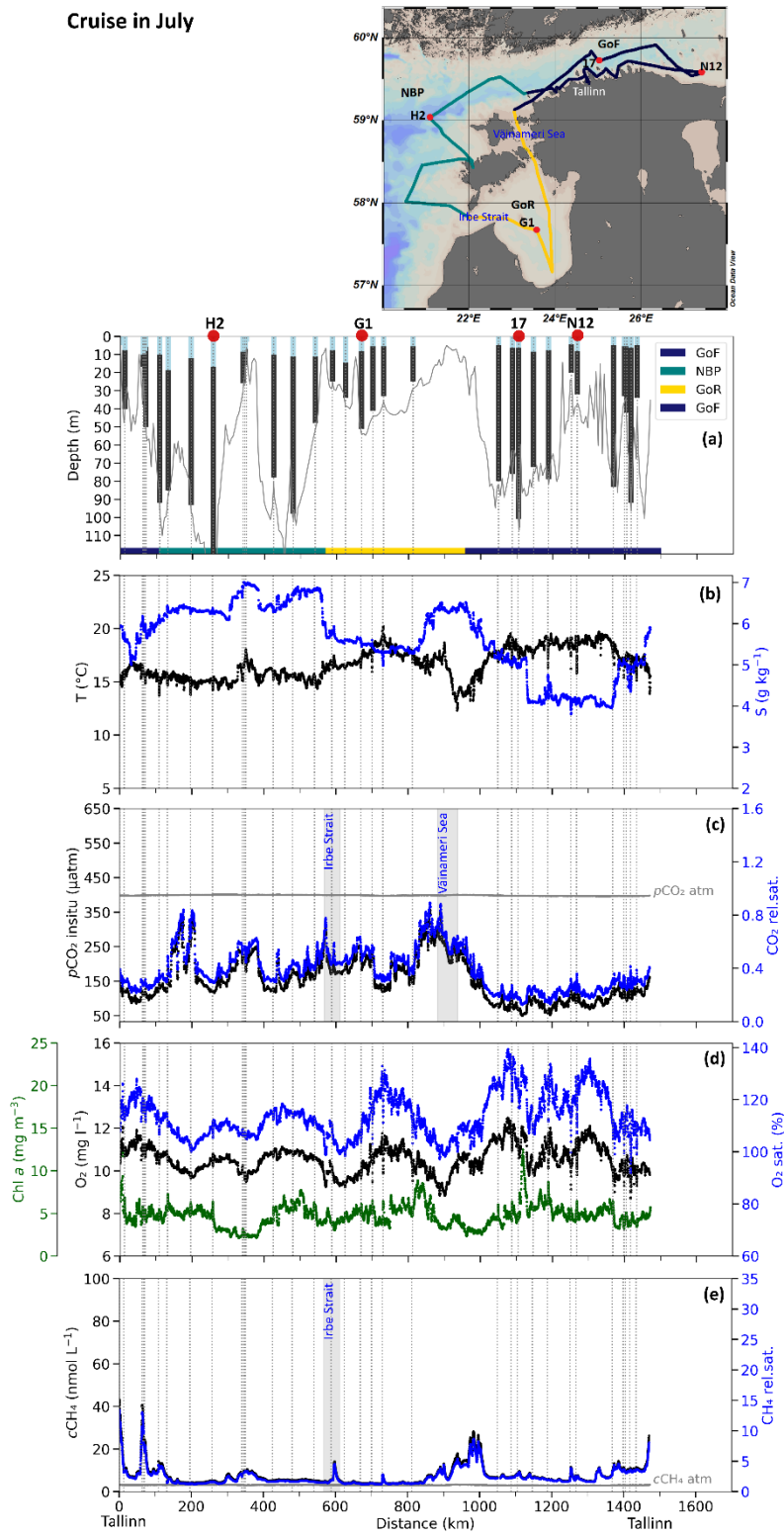
Figure 7: July monitoring cruise (9-13 July): The trajectory is shown on the map and on panel (a) UML depth (light blue bars) and the water column extent below the UML (dark blue bars); vertical grey dashed lines indicate the locations of monitoring stations, the locations of the most characteristic stations of the sub-basins are denoted with red dots. (b) Spatial variability of temperature (left y-axis) and salinity (right y-axis), (c) CO_2 partial pressure (left y-axis) and relative saturation (right y-axis), (d) Chl *a* (left y-axis), dissolved oxygen concentration (left y-axis) and saturation (right y-axis), and (e) CH_4 concentration (left y-axis) and relative saturation (right y-axis). The x-axis denotes the distance (in km) from the start of the monitoring cruise (Tallinn).

Cruise in August

Figure 8: August monitoring cruise (22-27 August): The trajectory is shown on the map and on panel (a) UML depth (light blue bars) and the water column extent below the UML (dark blue bars); vertical grey dashed lines indicate the locations of monitoring stations, the locations of the most characteristic stations of the sub-basins are denoted with red dots. (b) Spatial variability of temperature (left y-axis) and salinity (right y-axis), (c) CO_2 partial pressure (left y-axis) and relative saturation (right y-axis), (d) Chl a (left y-axis), dissolved oxygen concentration (left y-axis) and saturation (right y-axis), and (e) CH_4 concentration (left y-axis) and relative saturation (right y-axis). The x-axis denotes the distance (in km) from the start of the monitoring cruise (Tallinn). In August, cCH_4 signals in the river estuaries and coastal areas were extreme in comparison with the rest of the data, and these signals were cut on the panel to 100 nmol L^{-1} to properly display the structure within low-concentration areas.

Cruise in October
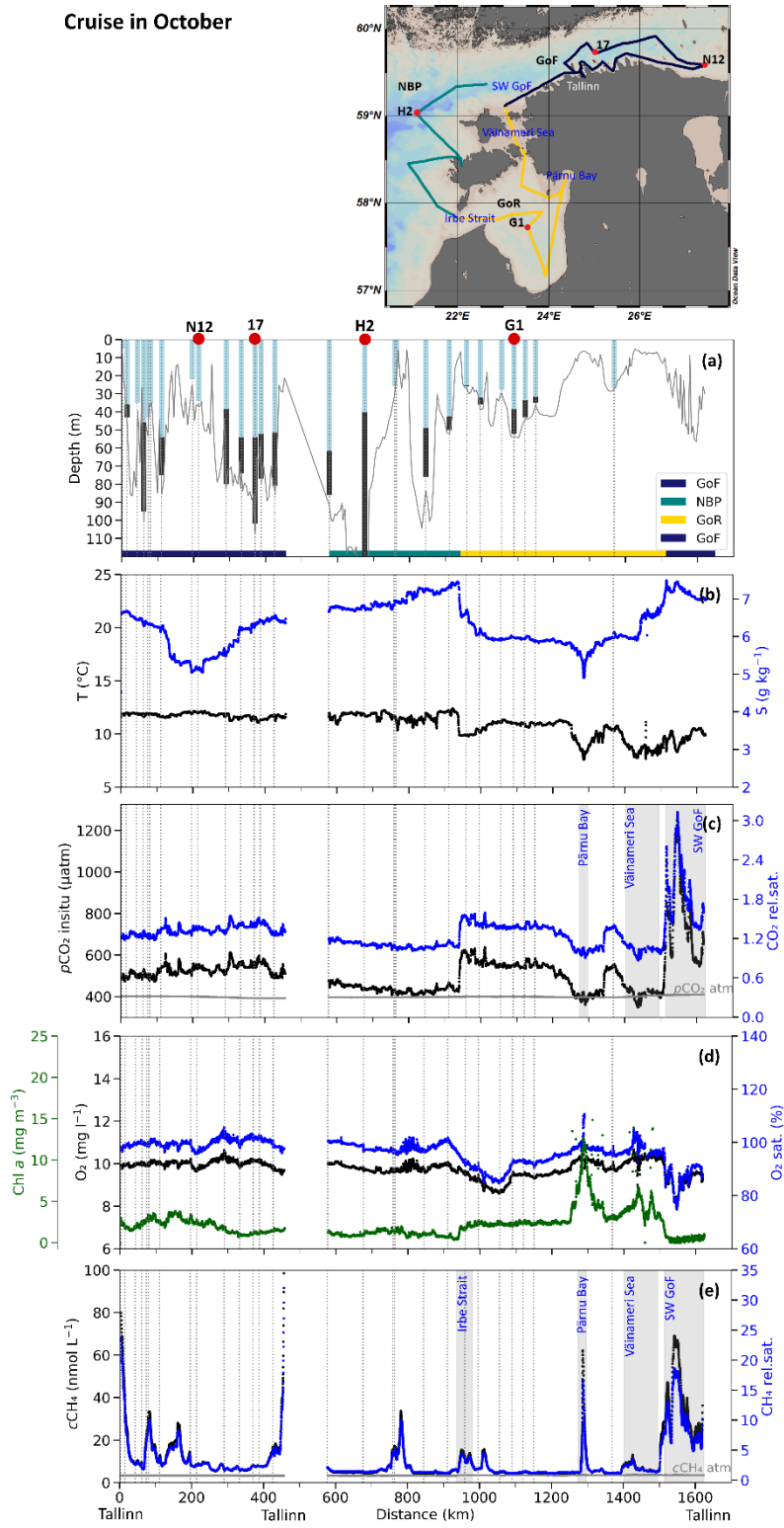
Figure 9: October monitoring cruise (22-28 October): The trajectory is shown on the map and on panel (a) UML depth (light blue bars) and the water column extent below the UML (dark blue bars); vertical grey dashed lines indicate the locations of monitoring stations, the locations of the most characteristic stations of the sub-basins are denoted with red dots. (b) Spatial variability of temperature (left y-axis) and salinity (right y-axis), (c) CO_2 partial pressure (left y-axis) and relative saturation (right y-axis), (d) Chl a (left y-axis), dissolved oxygen concentration (left y-axis) and saturation (right y-axis), and (e) CH_4 concentration (left y-axis) and relative saturation (right y-axis). The x-axis denotes the distance (in km) from the start of the monitoring cruise (Tallinn). In October, cCH_4 signal in the coastal areas was extreme in comparison with the rest of the data, and this signal was cut on the panel to 100 nmol L^{-1} to properly display the structure within low-concentration areas. Note different scale for CO_2 partial pressure and relative saturation in comparison with the rest of the cruises.

4.3 Seasonal variability

Seasonal variability of pCO_2 in 2018 (Fig. 10d) follows the general seasonal course in all analysed sub-basins (Table 1) with oversaturation in autumn-winter (average relative CO_2 saturation 1.2) and undersaturation in spring-summer (average relative CO_2 saturation 0.5) high values in winter, a decrease in spring, a minimum in late spring, and an increase in autumn (Table 1). The pCO_2 decrease in spring coincidences with the highest Chl a and dissolved oxygen concentrations in April. Based on decreased Chl a concentrations from mid-April to the end of May (Fig. 10e; Table 1), the early-summer minimum of phytoplankton biomass was evident. It is also at the end of May – early June when the pCO_2 seasonal minimum in all sub-basins appeared (Table 1). During midsummer, relatively high Chl a concentrations were recorded (Fig. 10e; Table 1) and dissolved oxygen concentrations stayed moderately oversaturated. pCO_2 values increased from July on, reaching oversaturation almost everywhere along the cruise track by the October cruise. No second pCO_2 minimum during summer nor a relative maximum between the two usually expected minima in spring and late summer were detected.

For the evaluation of the seasonal course of surface water methane concentrations, cCH_4 median values were analysed (Fig. 10h and Table 1). In all three sub-basins, the highest median concentrations of 13.7 nmol L^{-1} in the GoR, 11.5 nmol L^{-1} in the GoF and 7.6 nmol L^{-1} in the NBP were determined in April (note we do not have winter data), after which the concentrations started to decrease. The minimum level was reached in the GoF and GoR in July (median concentrations were 7.9 nmol L^{-1} and 4.5 nmol L^{-1}, respectively) and in the NBP in August (3.9 nmol L^{-1}). It was followed by an increase in concentrations by October, but the values did not reach yet the levels observed in April.

Although high cCH_4 values represent only a small part of acquired data, it is worthwhile to mark some seasonal changes in variability. The highest cCH_4 variations were observed in May, August and October in the GoF and in April, May and August in the GoR. It shows that although the average seasonal course in the GoF and GoR was similar to the NBP, regions existed in the GoF and GoR with locally high methane concentrations (extremes exceeding 100 nmol L^{-1}).
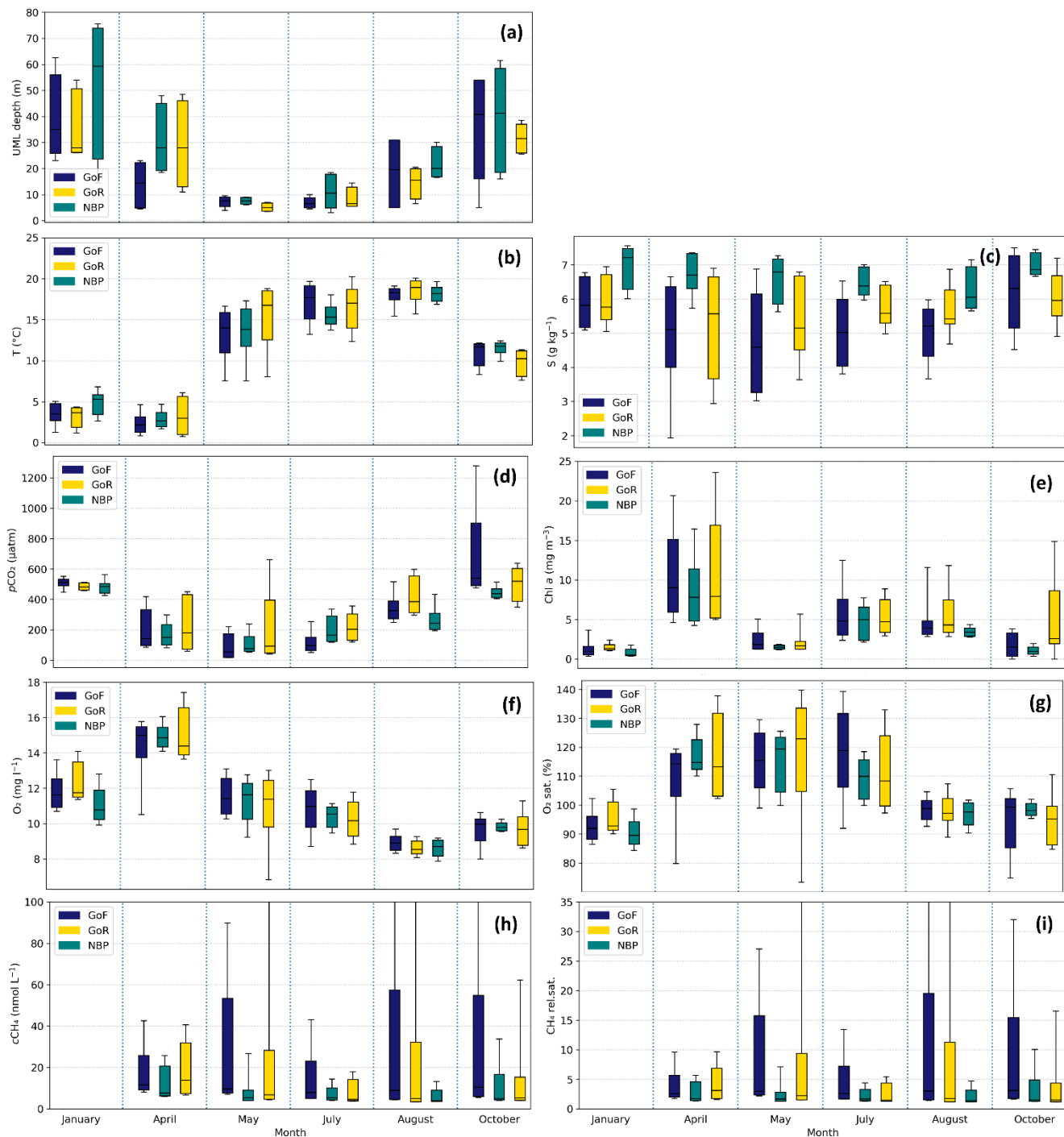
Figure 10: Median and 5/95 percentile values of (a) UML depth, (b) temperature, (c) salinity, (d) CO₂ partial pressure, (e) Chl *a*, (f) dissolved oxygen and (g) saturation, (h) CH₄ concentration and (i) relative saturation. Whiskers denote min and max values. In May, August and October cruises, *c*CH₄ signals in the river estuaries and coastal areas were extreme in comparison with the rest of the

data, and these signals are not seen on the plot (y-axis maximum is 100 nmol L^{-1} to properly display the pattern in low-concentration areas).

Table 1. Median / mean values of UML depth, temperature (T), salinity (S), CO_2 partial pressure (pCO_2), Chl *a*, dissolved oxygen (O_2) and saturation (O_2 sat.),

435   CH_4 concentration (cCH_4) and relative saturation (CH_4 rel.) for the Estonian sea area sub-basins in 2018.

		UML (m)	T (°C)	S (g kg^{-1})	pCO_2 (µatm)	Chl *a* (mg m^{-3})	O_2 (mg l^{-1})	O_2 sat. (%)	cCH_4 (nmol L^{-1})	CH_4 rel. sat. (%)
GoF	Jan	35 / 38	3.5 / 3.5	5.8 / 5.9	511 / 511	1.0 / 1.0	11.6 / 11.7	92 / 92	–	–
	Apr	15 / 15	2.2 / 2.2	5.1 / 5.1	141 / 178	9.0 / 9.7	15.0 / 14.9	114 / 112	11.5 / 13.8	2.5 / 3.0
	May	8 / 7	14.0 / 13.9	4.6 / 4.7	53 / 70	1.8 / 2.0	11.4 / 11.5	115 / 116	9.5 / 15.4	3.0 / 4.7
	Jul	7 / 7	17.7 / 17.4	5.0 / 4.9	97 / 102	4.8 / 5.0	11.0 / 10.9	119 / 119	7.9 / 9.9	2.6 / 3.2
	Aug	20 / 20	18.3 / 18.2	5.2 / 5.1	326 / 327	3.9 / 4.0	8.9 / 8.9	99 / 99	8.8 / 17.7	3.0 / 6.0
	Oct	41 / 40	11.7 / 11.4	6.3 / 6.2	540 / 580	1.5 / 1.7	10.0 / 9.8	99 / 97	10.5 / 17.9	3.1 / 5.2
NBP	Jan	59 / 55	5.3 / 5.1	7.2 / 7.1	484 / 480	0.5 / 0.6	10.8 / 10.8	90 / 90	–	–
	Apr	28 / 30	2.7 / 2.7	6.7 / 6.7	149 / 158	7.8 / 7.8	14.9 / 14.9	115 / 115	7.6 / 9.3	1.7 / 2.1
	May	8 / 8	13.8 / 13.9	6.8 / 6.7	75 / 86	1.5 / 1.5	11.6 / 11.5	119 / 118	5.4 / 6.1	1.7 / 1.9
	Jul	11 / 11	15.3 / 15.4	6.4 / 6.5	165 / 179	5.0 / 4.6	10.5 / 10.4	110 / 110	5.3 / 6.0	1.7 / 1.9
	Aug	20 / 21	18.2 / 18.2	6.1 / 6.1	243 / 250	3.4 / 3.4	8.7 / 8.7	98 / 98	3.9 / 4.5	1.3 / 1.5
	Oct	41 / 39	11.8 / 11.7	6.9 / 7.0	436 / 438	1.0 / 1.0	9.8 / 9.8	98 / 98	4.9 / 6.7	1.5 / 2.0
GoR	Jan	28 / 34	3.6 / 3.4	5.8 / 5.8	482 / 483	1.3 / 1.4	11.7 / 12.1	93 / 94	–	–
	Apr	28 / 29	3.0 / 3.0	5.6 / 5.4	180 / 227	7.9 / 9.2	14.4 / 14.8	113 / 115	13.7 / 16.6	3.1 / 3.7
	May	5 / 5	16.8 / 16.4	5.2 / 5.3	93 / 148	1.7 / 1.7	11.4 / 11.3	123 / 121	6.7 / 12.4	2.2 / 4.0
	Jul	7 / 8	17.0 / 17.0	5.6 / 5.7	204 / 210	4.7 / 4.9	10.2 / 10.2	108 / 110	4.5 / 6.1	1.4 / 2.0
	Aug	16 / 15	18.9 / 18.9	5.4 / 5.6	385 / 413	4.3 / 4.8	8.5 / 8.6	97 / 98	5.0 / 10.2	1.8 / 3.6
	Oct	32 / 31	10.2 / 10.0	6.0 / 6.0	519 / 495	2.6 / 3.5	9.7 / 9.7	95 / 94	5.3 / 7.3	1.5 / 2.0

4.4 Estimates of the air-sea CO_2 and CH_4 fluxes

The air-sea CO_2 and CH_4 fluxes calculated for every research cruise were seasonally averaged so that winter is characterised
440 by the cruise in January, spring – April and May, summer – July and August, and autumn – October (Tables 2 and 3; Fig. 11).

Table 2. Seasonal and annual CO_2 flux estimates with standard deviations for the Estonian sub-basins and sea area in 2018.

	Seasonal median / mean CO_2 fluxes (g C m^{-2} day^{-1}; ± standard deviation)			
	GoF	**NBP**	**GoR**	**Estonian sea area**
Winter	0.06 / 0.07 (±0.04)	0.02 / 0.02 (±0.02)	0.08 / 0.07 (±0.05)	0.04 / 0.05 (±0.04)
Spring	-0.30 / -0.36 (±0.23)	-0.14 / -0.13 (±0.09)	-0.22 / -0.21 (±0.13)	-0.21 / -0.26 (±0.20)
Summer	-0.11 / -0.11 (±0.06)	-0.16 / -0.17 (±0.08)	-0.04 / -0.02 (±0.13)	-0.10 / -0.10 (±0.11)
Autumn	0.29 / 0.32 (±0.20)	0.04 / 0.04 (±0.03)	0.13 / 0.14 (±0.14)	0.16 / 0.19 (±0.19)
Annual mean	-0.02	-0.06	-0.005	-0.03

Table 3. Seasonal CH_4 flux estimates with standard deviations for the Estonian sub-basins and sea area in 2018.

	Seasonal median / mean CH_4 fluxes (mg C m^{-2} day^{-1}; ± standard deviation)			
	GoF	**NBP**	**GoR**	**Estonian sea area**
Winter	–	–	–	–
Spring	0.20 / 0.24 (±0.17)	0.03 / 0.05 (±0.06)	0.12 / 0.26 (±0.31)	0.14 / 0.20 (±0.22)
Summer	0.14 / 0.43 (±0.99)	0.05 / 0.06 (±0.07)	0.04 / 0.18 (±0.46)	0.07 / 0.25 (±0.71)
Autumn	0.37 / 0.74 (±0.77)	0.07 / 0.10 (±0.12)	0.07 / 0.21 (±0.29)	0.18 / 0.39 (±0.59)

445

The CO_2 flux estimates (Table 2) show that the Estonian sea area was a source of atmospheric CO_2 (positive flux) during winter and autumn and a sink (negative flux) during spring and summer 2018. What stands out is that the standard deviations are of the same order of magnitude as the estimated average fluxes. The observed spatial variability was larger in the GoR and GoF than in the NBP (Figs. 4-9). The annual mean flux (estimated as an arithmetic average of the four seasonal flux estimates) 450 in the NBP was -0.06 g C m^{-2} d^{-1}, in the GoF -0.02 g C m^{-2} d^{-1} and in the GoR -0.005 g C m^{-2} d^{-1}.

The CH_4 flux estimates (Table 3) show that the Estonian sea area was a source of atmospheric CH_4 during spring, summer and autumn (no data for winter). Note that the standard deviations of flux estimates exceeded the resulting average fluxes during summer and autumn. As with CO_2 fluxes, the spatial variability of observed CH_4 fluxes was larger in the GoR and GoF than 455 in the NBP (Fig. 11).
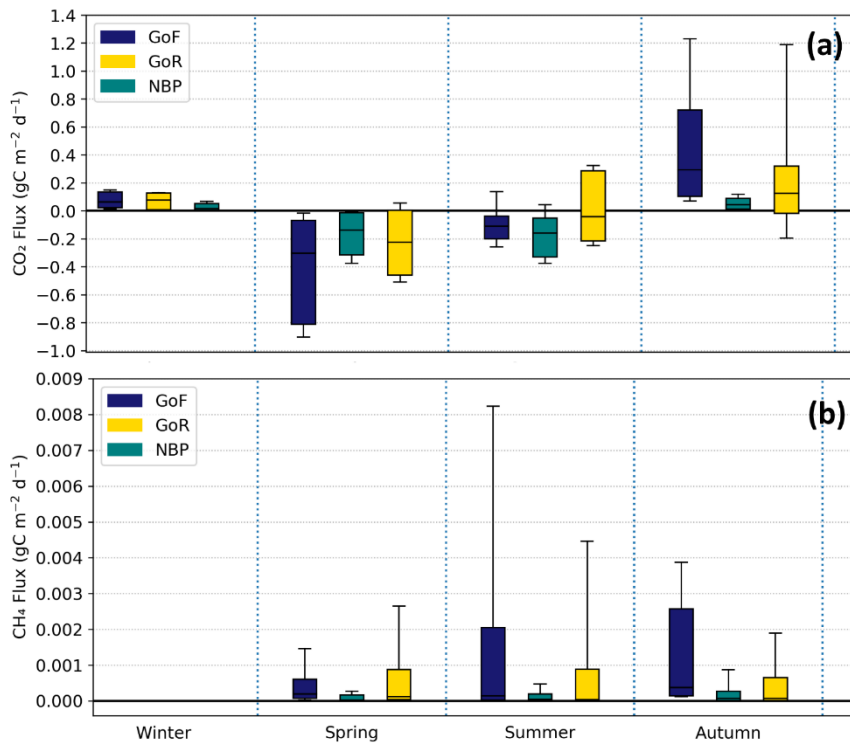
Figure 11: Seasonal median air-sea (a) CO₂ and (b) CH₄ flux estimates in the three analysed sub-basins of the north-eastern Baltic Sea in 2018. The flux is positive for the transport from the sea to the atmosphere, while negative values refer to the transport from the atmosphere to the sea.

5 Discussion

The first extensive trace gases study was conducted to describe spatial patterns and seasonal dynamics of CO_2 and CH_4 in the north-eastern Baltic Sea area~~, including the GoR~~. ~~Physical forcing and hydrographic/biological background in the study year (2018) were analysed to explain the observed patterns in pCO_2 and cCH_4.~~ The main focus was on the southern Gulf of Finland and the Gulf of Riga, as earlier studies addressed measurements from the Baltic Proper and the western Gulf of Finland (e.g. Schneider et al., 2014; Schneider and Müller, 2018; Gülzow et al., 2013).

5.1 Patterns of variability in the southern GoF and GoR

5.1.1 pCO_2 distribution patterns

Cruises of R/V Salme covered both the offshore and the coastal areas in the GoF and GoR, with the most prominent local pCO_2 peaks in the shallow coastal sea areas. These local maxima were mostly linked to ~~coastal physical processes such as~~

river bulges, coastal upwelling events, fronts and vertical mixing reaching the seabed, but also to phytoplankton distribution patterns influenced by meteorological and hydrographic conditions.

Rivers are the major carbon source ~~of carbon~~, including dissolved inorganic carbon for the coastal ocean (Dai et al., 2022) and
475 the Baltic Sea (Kuliński and Pempkowiak, 2011). In the GoF, ~~river discharge is mainly concentrated in the easternmost part of the gulf, and~~ the largest freshwater source along the R/V track was the Narva River (Stålnacke et al., 1999) ~~visited in April, May-June and August. The~~Its influence ~~of Narva River waters~~, identified by a simultaneous local decrease in salinity and increase in pCO$_2$, was largest in August (Fig. 8c), when CO$_2$ concentrations locally exceeded saturation level, while in April and May-June, only a slight increase in pCO$_2$ relative to the surrounding waters was observed. In the GoR, river discharge is
480 concentrated in the southern and eastern parts of the gulf (Yurkovskis et al., 1993). ~~Observations close to the largest river discharges in the south of GoR were conducted in May-June, July, August and October, and in the shallow Pärnu Bay under the influence of the Pärnu River discharge in April, May-June, August and October.~~

~~The influence of Narva River waters, identified by a simultaneous local decrease in salinity and increase in pCO$_2$, was largest
485 in August (Fig. 8c), when CO$_2$ concentrations locally exceeded saturation level, while in April and May-June, only a slight increase in pCO$_2$ relative to the surrounding waters was observed.~~ The influence of large rivers of the southern GoR was detected by a slight decrease in salinity in May-June and July, but a simultaneous increase in pCO$_2$ was observed only in May-June. The largest peaks, which could be linked to the river discharges, were associated with the Pärnu River, especially in April and May-June, when the background levels of pCO$_2$ in the adjacent regions were already low. Thus, the river waters
490 influenced the observed pCO$_2$ patterns remarkably in the shallow and semi-enclosed Pärnu Bay and less in other areas. ~~Probably, the research vessel track did not reach the river bulges properly in the southern GoR, or their influence was not seen offshore since the riverine waters were mostly transported along the coast (e.g. Lips et al., 2016b) and an anticyclonic river bulge was not formed as suggested by a modelling study (Soosaar et al., 2016).~~

495 Upwelling is the most prominent mesoscale process in the elongated GoF (Myrberg and Andrejev, 2003), where upwelling events along the southern coast are associated with north-easterly and easterly winds (Lips et al., 2009; Kikas and Lips, 2016). Winds supporting upwelling along the GoF southern coast dominated in October and also, though with lower wind speed, in July and late May. ~~In October, up to three times higher pCO$_2$ values than the background were recorded in the upwelled waters.~~ In October, b~~B~~ased on a comparison of salinity and temperature in the surface layer in the upwelling area and vertical profiles
500 registered at the monitoring stations two days earlier, the upwelled waters mostly originated from the water layer of 65-75 m, i.e. the halocline. Most likely, the observed extreme pCO$_2$ values were caused by the relatively deep origin and the impact of the seabed when these waters were brought to the surface along the GoF slope.

In ~~the~~ a case of upwelling in the Gotland basin in July-August 2016, a very sharp increase in pCO_2 was measured, although the absolute values were lower than in our study (Jacobs et al., 2021). The authors evaluated the air-sea fluxes of CO_2 due to this upwelling event and showed that the CO_2 flux, expected to be directed from air into the sea in August, was reduced and even reversed due to upwelling. ~~High variability of wind conditions, sea surface temperatures and other factors make it difficult to estimate the total impact of upwelling events on total air sea fluxes of CO_2 precisely. However,~~ Kuss et al. (2006) have suggested that roughly 20% of the annual CO_2 uptake in the central Arkona Sea could be balanced by CO_2 release during occasional upwelling events in the coastal areas, also considering seasonal differences in their impact. Similarly, Norman et al. (2013) estimated that upwelling events could possibly decrease the Baltic Sea's annual average CO_2 uptake by up to 25%. In 2018, ~~the~~ winds favouring upwelling along the northern coast of GoF prevailed. However, we detected the upwelling events in the western GoF along the southern coast during cruises in late May and October. The highest pCO_2 values were recorded in upwelled waters in October when likely autumn mixing contributed to the vertical exchange, but it ~~and~~ did not trigger production.

The seasonal course in pCO_2 in the surface layer is mainly controlled by the primary production in spring/summer and entrainment of waters with high pCO_2 due to remineralisation processes during mixed layer deepening in fall (e.g. Schneider and Müller, 2018). The seasonal succession of phytoplankton, however, could be at different stages of development due to varying meteorological and hydrographic background along the 1500 km long measurement track (e.g. Seppälä and Balode, 1999; Lips et al., 2014). ~~A prominent example of such spatial variability was revealed in April when pCO_2 and Chl a were negatively correlated.~~ In April t~~T~~he highest pCO_2 values, corresponding to the saturation level, observed in the parts of GoR and GoF coincided with lower than the background Chl a and oxygen concentrations (Fig. 5c and d). The lowest pCO_2 values were recorded in shallow areas with a warm surface layer with high Chl a concentrations. It is remarkable that in areas of high pCO_2, the sea surface temperature was 1-2 °C, meaning below the temperature of the maximum density of approximately 2.5 °C, and the water column was almost fully mixed, e.g. ~~The latter was evident from the vertical profiles registered at the monitoring stations and relatively high surface salinity, especially.~~ in the western and central GoR. ~~It can be assumed that when the bloom reached its peak, low pCO_2 could also be recorded in this area.~~

Like the stratification and bloom development in spring, the upper mixed layer deepening and stratification decay could shape the pCO_2 distribution patterns in the surface layer in late summer and autumn. By the August cruise, the upper mixed layer has been deepened to almost 30 m from the values of around 10 m in July. This resulted in high pCO_2 values in shallow areas (Fig. 8c), where the mixing has reached the bottom layer. ~~It is interesting that a similar pattern was not evident in October.~~However, ~~T~~the areas with higher pCO_2 values during summer cruises had CO_2 levels in October lower than in the deeper areas, where the mixing reached the near-bottom layer later, leaving less time for equilibration with the atmosphere in these deeper areas.

~~The described seasonal pattern was observed in the Väinameri Sea (northern GoR) with an average depth of 5–10 m. However,~~ ~~this area is very dynamic and~~ ~~relatively strong gradients of oceanographic variables (salinity, nutrients, etc.) are observed~~ ~~(Suursaar et al., 2001).~~ We suggest the following processes responsible for the observed seasonal pattern in the Väinameri Sea (northern GoR) with an average depth of 5-10 m and relatively strong gradients of oceanographic variables ~~(salinity, nutrients, etc.) are observed~~ (Suursaar et al., 2001). In April, pCO_2 levels were lower than in the adjacent deeper areas due to a warm surface layer and an earlier start of the spring bloom since the phytoplankton mixing depth in shallow areas is determined by the bottom depth and not vertical stratification (Townsend et al., 1994). In late May and July, the highest pCO_2 values were measured at the saltier side of the salinity front in the Väinameri Sea, likely ~~. We suggest that these maxima were~~ favoured by weaker vertical stratification and, consequently, stronger vertical fluxes at the denser side of the fronts (e.g., Kahru et al., 1984). In August, the higher pCO_2 values in the shallow Väinameri Sea were likely related to the vertical mixing, and in October, when oversaturation was observed almost along the entire R/V track, pCO_2 was higher in other, deeper areas where the vertical flux (due to continuing upward mixing of deep, CO_2-rich waters) was still at a higher level, while a larger fraction of the CO_2 from the near-bottom layer had already evaded from the Väinameri Sea.

Another area where saltier Baltic Proper and fresher GoR waters meet and the front develops, is the Irbe Strait, conveying most of the GoR water exchange with the NBP (Lilover et al., 1998). Locally, the lowest pCO_2 was measured in connection to the Irbe front in April, probably due to the development of vertical stratification supporting the spring bloom, while in the GoR, stratification was weak, and the bloom had not started yet. Contrarily, a slight local peak of pCO_2 in July could be caused by more intense vertical transport of sub-surface waters at the front.

5.1.2 cCH$_4$ distribution patterns

cCH$_4$ was oversaturated in the surface layer during the whole study period, which is typical for the Baltic Sea (Gülzow et al., 2013), with prominent local peaks in the GoF and GoR. These peaks can be related to the same physical processes as the local maxima in pCO_2 spatial distribution. However, two major peculiarities of cCH$_4$ distribution can be noticed – the local maximum values were more than an order of magnitude larger than the background cCH$_4$ level, and these prominent maxima were confined to the shallow areas. Although these peaks were not always observed in all shallow areas ~~Almost in all shallow bays, which were visited during different cruises in the GoF and GoR, and also in the Tagalaht Bay in the NBP in October, high peaks of cCH$_4$ were recorded.~~ , t~~T~~his pattern agrees with the earlier results that methane concentrations and variability are high in shallow coastal areas (Roth et al., 2022; Borges et al., 2016).

Rivers have been identified as potentially strong sources of CH$_4$ in the Baltic Sea (Myllykangas et al., 2020). ~~. Rivers~~ receiving~~e~~ CH$_4$ from soils, groundwater, wetlands, and floodplains in the watershed (De Angelis and Lilley, 1987; Richey et al., 1988). In April and May, elevated cCH$_4$ was measured near the Narva River mouth. However, the enhanced cCH$_4$ was also measured along the shallow coastal sea towards the west from the Narva River mouth. Similar distribution in August, with the maximum

not at the mouth area but in the west, suggests that the river discharge was transported along the coast, as it could occur during summer months (Laanearu and Lips, 2003) or the shallowness and influence of sediments was the main factor creating this cCH_4 maximum. The latter suggestion or a combination of both are likely explanations, since the water column was fully mixed along the ship track in this area.

575

Notable cCH_4 spatial variability emerged in the shallow Pärnu Bay, while only slightly higher than background cCH_4 values were measured in the southern GoR, close to the largest river discharges, most probably, as suggested above, due to the absence of the predicted river bulge (Soosaar et al., 2016). Probably, the research vessel track did not reach the river bulges properly in the southern GoR, or their influence was not seen offshore since the riverine waters were mostly transported along the coast (e.g. Lips et al., 2016b) and an anticyclonic river bulge was not formed as suggested by a modelling study (Soosaar et al., 2016). The highest cCH_4 peaks in the Pärnu Bay were observed in May and August (approximately 200 nmol L^{-1}), while in October, the peak was not so prominent, although the river discharge was larger than in summer months. In shallow coastal areas, high methane emissions have been linked to the amount of organic matter in the sediment and water temperature (e.g. Heyer and Berger, 2000). Also, local maxima of cCH_4 were more pronounced in the Pärnu Bay in comparison with the areas close to the Narva River mouth. We suggest this pattern is related to the shallowness and semi-enclosed shape of the Pärnu Bay and not directly to the amount and changes in the river runoff.

The seafloor in most of the shallow bays is characterised by clay and mud or mixed sediments (mud and sand; EMODnet Geology), which are potential internal sources of methane (e.g. Humborg et al., 2019). This explains why cCH_4 peaks were recorded in these shallow areas where the water column was usually mixed until down to the seabed. In October, when high cCH_4 values were also measured in the deeper Kolga Bay and along the relatively deep south-western GoF (Fig. 9e), these findings can be related to autumn vertical mixing and an intense upwelling event. A similar impact of upwelling has also been shown by earlier measurements in the Baltic Sea (Gülzow et al., 2013; Jacobs et al., 2021) and other coastal sea areas (e.g. Kock et al., 2008). It is noteworthy that our data show the impact of upwelling on surface CO_2 and CH_4 concentrations in fall, when upwelling was identified by salinity rather than temperature. Previous studies (Gülzow et al., 2013; Schneider et al., 2014; Jacobs et al., 2021) use the drop in sea surface temperature as an indicator for upwelling and upwelling-induced greenhouse gas fluxes, which bears the risk of underestimating the importance of upwelling for locally enhanced CO_2 and CH_4 fluxes in the Baltic in fall.

600

Elevated cCH_4 was almost always measured in the Väinameri Sea and can be explained by vertical mixing and resuspension of bottom sediments. Resuspension events occur due to wind mixing and waves but also due to frequently appearing strong currents in the straits (Suursaar et al., 2001;). These strong currents are forced by wind-induced differences in the sea level between the adjacent basins (Otsmann et al., 2001). However, the detected cCH_4 peaks in the Väinameri Sea were not as strong

605   as in the Pärnu Bay, ~~for instance,~~ and in October, a much higher cCH$_4$ peak was measured just outside of the Väinameri in the

upwelled waters in the south-western GoF (concentrations reached up to 70 nmol L^{-1}; Fig. 9e).

610   In the Irbe Strait, local cCH$_4$ maxima were also frequently observed. However, their locations were different from the observed

pCO$_2$ extrema. We suggest that also here, the cCH$_4$ maxima were related to the shallowest spots along the vessel track (either

close to the Kolka or Sõrve peninsulas) and not to the Irbe front, as was ~~suggested~~ observed for the observed pCO$_2$ peaks.

~~Rivers have been identified as potentially strong sources of CH$_4$ in the Baltic Sea (Myllykangas et al., 2020). Rivers receive~~

615   ~~CH$_4$ from soils, groundwater, wetlands, and floodplains in the watershed (De Angelis and Lilley, 1987; Richey et al., 1988).~~
~~In April and May, elevated cCH$_4$ was measured near the Narva River mouth. However, the enhanced cCH$_4$ was also measured~~
~~along the shallow coastal sea towards the west from the Narva River mouth. Similar distribution in August, with the maximum~~
~~not at the mouth area but in the west, suggests that the river discharge was transported along the coast, as it could occur during~~
~~summer months (Laanearu and Lips, 2003) or the shallowness and influence of sediments was the main factor creating this~~
620   ~~cCH$_4$ maximum. The latter suggestion or a combination of both are likely explanations, since the water column was fully~~
~~mixed along the ship track in this area.~~

~~Notable cCH$_4$ spatial variability emerged in the shallow Pärnu Bay, while only slightly higher than background cCH$_4$ values~~
~~were measured in the southern GoR, close to the largest river discharges, most probably, as suggested above, due to the absence~~
625   ~~of the predicted river bulge (Soosaar et al., 2016). The highest cCH$_4$ peaks in the Pärnu Bay were observed in May and August~~
~~(approximately 200 nmol L^{-1}), while in October, the peak was not so prominent, although the river discharge was larger than~~
~~in summer months. In shallow coastal areas, high methane emissions have been linked to the amount of organic matter in the~~
~~sediment and water temperature (e.g. Heyer and Berger, 2000). Also, local maxima of cCH$_4$ were more pronounced in the~~
~~Pärnu Bay in comparison with the areas close to the Narva River mouth. We suggest this pattern is related to the shallowness~~
630   ~~and semi-enclosed shape of the Pärnu Bay and not directly to the amount and changes in the river runoff.~~

In summary, physically disturbed organic-rich sediments, river plumes, and upwelling were identified as processes causing

hot spots of methane emission. While methane from undisturbed organic-rich sediments usually does not surpass effective

anaerobic and aerobic methane oxidation in the upper sediment (e.g. Knittel and Boetius, 2009), physical shear stress can lead

635   to the release of methane from the upper sediment layer. ~~As a consequence,~~ Borges et al. (2016) suggested water depth as a

proxy for methane flux over organic-rich sediments in the North Sea. ~~Loads from rivers are expected to cause the highest~~
~~methane inputs in summer because of enhanced organic matter turnover and methanogenesis under warmer conditions, in~~

accordance with our findings. Similarly, ~~O~~our data support the importance of processes in shallow areas~~water processes~~ for assessing~~the assessment of~~ the CH$_4$ fluxes from the Baltic (and other marginal seas) to the atmosphere.

5.2 Comparison of seasonal variability between the basins

The temporal variations in pCO$_2$ in the surface layer of the NBP, GoF and GoR in 2018 followed, in general, the known seasonal course~~: high values in winter, low values in spring summer and a subsequent increase in autumn~~ (Thomas and Schneider, 1999; Schneider and Müller, 2018). In the Gotland Sea, the pCO$_2$ seasonal amplitude ~~varied~~ between 100-550 µatm has been registered (Schneider and Müller, 2018). In our study, t~~T~~he seasonal amplitude of pCO$_2$ was similar in all basins, with a slightly larger range in the GoF (50-1200 µatm). This higher amplitude is likely, at least in part, a result of the lower alkalinities in the GoF, which result in a higher pCO$_2$ change per amount of fixed carbon (e.g. Kuliński et al., 2017). The seasonal pCO$_2$ minimum in all basins ~~did not coincide with the peak of the spring phytoplankton bloom but~~ appeared at the end of May when surface layer Chl a concentrations were already relatively low, as a result of the cumulative nature of the imprint of primary production on the inorganic carbon system. Our data did not reveal an increase in pCO$_2$ between the spring bloom and the cyanobacteria bloom in midsummer, which has been reported based on measurements with a higher temporal resolution (e.g. Schneider et al., 2014).

~~pCO$_2$ seasonality is mainly controlled by biological activity in combination with the vertical mixing and stratification of the water column (Schneider et al., 2014).~~ In ~~both basins,~~ the GoF and the GoR, Chl a concentrations in spring (Fig. 10e, Table 1) were higher than in the NBP, which is in accordance with the elevated nutrient concentrations in the GoF and GoR (HELCOM, 2018). However, a slightly higher average pCO$_2$ in the GoR during spring and summer could be related to the shallowness of this basin. Higher pCO$_2$ in the GoF in October and January can be explained by high biomass production in spring-summer and the specific hydrographic conditions supporting vertical transport and mixing of CO$_2$ from the deep layers in autumn-winter and during the upwelling events, in combination with the reduced buffering due to lower alkalinity in the GoF. High concentrations of inorganic carbon in the deep layers of the GoF result from the organic matter degradation in the presence of stratification in spring and summer and the advection of deep waters from the Baltic Proper (Lehtoranta et al., 2017). In late autumn and winter, collapses of vertical stratification could occur in the GoF (Liblik et al., 2013), resulting in the vertical transport of nutrients (and inorganic carbon) from the near-bottom layer to the surface layer (Lips et al., 2017). The high pCO$_2$ values attributed to upwelling in October in the GoF, also characterized by the lowest surface O$_2$ saturation of the entire survey, confirm active transport mechanisms of deep waters with strong biogeochemical indicators of mineralisation of organic matter (Fig. 9c).

Since the GoR is shallower than the GoF and without a permanent halocline, CO$_2$ accumulation and subsequent CO$_2$ flux from the GoR deep layer do not have a similar high potential in autumn-winter as in the GoF. However, the seasonal thermocline was stronger in spring-summer 2018 than on average due to high heat flux and calm wind conditions (Stoicescu et al., 2022).

A near-bottom hypoxic layer developed, and the autumn-winter mixing had not reached the seabed in the deeper central GoR yet by the cruise in October (Stoicescu et al., 2022, also Fig. 9a). ~~, and T~~this could be a reason that relatively low pCO$_2$ was measured in the GoR while upwelling-related high values were recorded in the south-western GoF.

675 ~~Our pCO$_2$ annual dynamics did not reveal~~In our study, the second pCO$_2$ minim~~um in summer (or an increase between two minima)~~a during ~~summer, which in the NBP have been reported to appear in early July (Schneider and Müller, 2018). This is~~ was not revealed most probably due to the long interval between cruises: 5 weeks between the cruises in late May–early June and mid-July and 5 weeks between the cruises in mid-July and the end of August. Summer cyanobacterial bloom in the GoF is usually starting at the end of June or early July (Lips and Lips, 2008). Based on our data from mid-July, calm wind conditions

680 and high sea surface temperature (median 17.7 °C, Table 1) favoured the bloom, which is also observable in an increase in Chl a concentration. Müller et al. (2021) showed that in 2018, in the Eastern Gotland Sea, the production was intense from the beginning of their study period, the 6th of July (surface water pCO$_2$ was already as low as around 100 µatm), and *Nodularia* sp peaked on the 24th of July, which is also the date of lowest pCO$_2$ values around 70 µatm. However, in the GoR, cyanobacteria biomass was three times lower in 2018 than in 2017 and a factor of two lower than the long-term mean (Kownacka et al.,

685 2022).

cCH$_4$ dynamics in 2018 in the NBP, GoF and GoR follow~~ed~~ the general seasonal cycle with the lowest methane concentrations in summer when~~.~~ thermal stratification ~~of the water column~~ hampers the methane transport ~~between the sea surface and~~from the deeper layers and~~. T~~ the surface water gets depleted ~~in methane~~ due to loss to the atmosphere by sea-air exchange, in part

690 driven by the temperature-induced decreasing solubility. ~~cCH$_4$ seasonality is controlled by the sediment organic matter content in combination with the stratification of the water column.~~ Gülzow et al. (2013) showed that the GoF surface water is characterised by elevated methane concentrations throughout the year (up to 22 nM in February) compared to ~~other~~ offshore Baltic Sea regions ~~(their study area did not cover the GoR)~~. In our study, the NBP summer minimum remained within the comparable range with Gülzow et al. (2013), but the GoF summer minimum was twice as high. Note, that we also covered the

695 shallow southern coastal sea areas of the GoF with remarkable local peaks, while the GoF sub-transect by Gülzow et al. (2013) was almost fully located in the central Gulf of Finland.

~~During summer, thermal stratification of the water column hampers the methane transport between the sea surface and the deeper layers. The surface water gets depleted in methane due to loss to the atmosphere by sea-air exchange, in part driven by~~

700 ~~the temperature-induced decreasing solubility.~~ Schmale et al. (2010) suggested that during summer, elevated methane concentrations are observable in the GoF water column up to a depth of 20–30 m. Aerobic methane production has also been demonstrated to contribute to the slight oversaturation of surface waters in the central Baltic Sea (Schmale et al., 2018; Stawiarski et al., 2019), but the clear link of methane peaks to shallow areas and episodes of mixing reaching the seafloor suggests that these processes are of minor importance in our study area.

705

~~In our study, the NBP summer minimum remained within the comparable range with Gülzow et al. (2013), but the GoF summer minimum was twice as high.~~ ~~We also covered the shallow southern coastal sea areas of the GoF with remarkable local peaks, while the GoF sub-transect by Gülzow et al. (2013) was almost fully located in the central Gulf of Finland and avoided shallow coastal waters.~~ Furthermore, the highest CH_4 concentrations observed in October 2018 in the south-western GoF could be a

710 consequence of the specific hydrographic conditions – a combined effect of strong upwelling and autumn mixing.

In the GoR, sediments have a high organic matter content, and the area undergoes intermittent seasonal hypoxia (Stoicescu et al., 2022). In the shallow areas, likely wind-induced mixing remains relevant for the transport of methane from the sediment, including the potential for sediment resuspension and mobilization of methane-enriched pore waters. In April, the highest

715 median cCH_4 was detected in the western and central parts of the GoR, where the water column was fully mixed down to the seabed. The seasonal stratification in the GoR during spring-summer 2018 was stronger than on average. It restricted vertical mixing and led to pronounced near-bottom oxygen depletion (Stoicescu et al., 2022) and probably to relatively low cCH_4 in the surface layer of the deeper GoR areas (where the seasonal thermocline existed). ~~Relatively low methane concentrations in October suggest that the autumn mixing had not yet reached the seabed in deep GoR areas by October.~~

720 **5.3 Air-sea gas exchange**

Several approaches have been used to assess whether the Baltic Sea is a sink or source of atmospheric CO_2, but no uniform consensus has been reached regarding the results (Dai et al., 2022). The estimation of fluxes on regional or global scales depends on the applied approaches, among them, whether pCO_2 data are calculated from other parameters (i.e. pH and total alkalinity) or direct pCO_2 measurements are conducted, model-based or remote sensing approaches used (e.g. Wesslander et

725 al., 2010; Schneider et al., 2014; Kuliński and Pempkowiak, 2011; Parard et al., 2017). In addition, most of the evaluations have been performed based on the data in the Baltic Proper (Gotland basin; e.g. Thomas and Schneider, 1999; Schneider et al., 2014), and only a few studies have included data from the north-eastern sea areas (e.g. Honkanen et al., 2020). The results of our study show no major differences in the behaviour between the analysed three basins, in general, except the high variability in the GoR and GoF that was likely observed since more shallow coastal areas were covered in these regions. It was also

730 pointed out by Gutiérrez-Loza et al. (2021) that the fluxes in the Baltic Sea coastal regions were larger than in the open sea area.

The CO_2 flux estimates (Table 2) show that the Estonian sea area was a source of atmospheric CO_2 during the winter and autumn and a sink during the spring and summer of 2018. Also, the estimates suggest that all studied sub-basins were CO_2

735 sinks on an annual basis. However, due to the high temporal and spatial variability and the fact that the 6 cruises were distributed unevenly across the year, with bi-monthly gaps between the measurements in autumn and winter, it cannot be conclusively defined whether the area is a source or a sink over the course of the year.

In our study, the estimated annual mean flux in the NBP was -0.06 g C m^{-2} d^{-1} (-1.8 mol m^{-2} yr^{-1}). Flux estimates for 2005,
2008 and 2009 by Schneider et al. (2014) showed that the central and northern Gotland basins act as a net sink for atmospheric
750   CO_2 with uptake rates ranging between -0.60 and -0.89 mol m^{-2} yr^{-1}. Several factors may account for these differences in flux
estimates. The summer of 2018 could have been more productive due to warm weather conditions. On the other hand, our
measurements covered the transition areas NBP–GoF and NBP–GoR, where the fluctuations in fluxes are greater than in
offshore areas analysed in the study by Schneider et al. (2014). Müller et al. (2021) concluded that their observations in the
eastern Gotland basin in July–August 2018 were representative for Baltic Sea cyanobacteria blooms in general, although the
755   pCO_2 levels in 2018 varied between the upper and lower ends of the conditions observed in previous years (Schneider and
Müller, 2018). Additionally, the difference in flux estimates might be caused by different parametrizations used. (Wesslander
et al., (2011) showed that the flux estimates in the coastal region off the east coast of Gotland differed by 64% depending on
the parametrization used. The differences in the estimated CO_2 fluxes using different parametrizations could be largest during
the winter months (October to February), as suggested by Gutiérrez-Loza et al. (2021).
760

The calculated annual mean fluxes in the GoF and GoR were smaller than in the NBP. An analysis of these values in more
detail (Table 2) reveals that CO_2 uptake during spring-summer was the greatest in the GoF (Fig. 11a). As a counterbalance to
summer absorption, the CO_2 release in October had a large impact on the estimates of the annual mean fluxes. In the NBP, the
impact of the autumn release was smaller (Table 2), but it was significant for the GoF and GoR annual mean flux estimates
765   due to the upwelling event along the southern coast of the GoF and shallower basin with mixing reaching the seabed in most
of the GoR.

The Baltic Sea is a source of atmospheric CH_4 and shows strong spatial and seasonal variations (Bange et al., 1994; Gülzow
et al., 2013). Also, the present dataset shows that the Estonian sea area is a source of atmospheric CH_4 during spring, summer
770   and autumn (Table 3; Fig. 11b). A considerable increase in the calculated methane flux was observed in August, as also pointed
out in the studydetected by Gülzow et al. (2013) who explained such ., whereas Ttheir study covered mostly the Baltic Sea

offshore areas and the increase was explained as a consequence of the transition to the regime of high wind velocities. Due to the upwelling event in October, methane outgassing in our study was most probably intensified in autumn (Jacobs et al., 2021). Our The calculated CH_4 fluxes in the NBP (Table 3; Fig. 11b) were much lower and much less variable than in the GoF and

775   GoR. The reason is similar, as discussed regarding the CO_2 fluxes – more shallow coastal areas were covered in the GoF and GoR than in the NBP.

For a robust flux estimate in the entire (north-eastern) Baltic Sea, understanding and monitoring of coastal processes seem to be mandatory in addition to measurements in the central Baltic – even when integrating over the surface area. On the other

780   hand, even few data from the NBP are likely representative of a very large area, given the error ranges.

6 Conclusions

Spatial patterns and seasonal dynamics of CO_2 and CH_4 were studied in the north-eastern Baltic Sea area. We observed that the southern GoF and GoR have considerably higher spatial variability and seasonal amplitude of surface layer pCO_2 and cCH_4 than measured in the Baltic Sea offshore areas (pCO_2 50-1200 µatm vs 100-550 µatm, respectively; cCH_4 80 vs 22 nmol L^{-1},

785   respectively). The main processes behind this high variability are coastal upwelling events, hydrographic fronts (e.g. Irbe front), mixing reaching the seabed and possible shifts in the timing of bloom events influenced by hydrography. On average, the CO_2 air-sea fluxes in the north-eastern Baltic Sea are similar between the sub-basins but with larger amplitudes in the coastal areas. However, regional variations in CO_2 dynamics also result in differences in annual flux estimates between the sub-basins.

790

Due to the observed high variability, it is recommended to continue similar high-resolution measurements in the coastal and offshore areas at least every season during the regular environmental monitoring cruises. It is essential for accurately evaluating the role of this region in the Baltic Sea carbon budget and to predict potential future changes due to anthropogenic/climatic pressures. Additionally, high-resolution pCO_2 measurements have a strong potential to contribute to eutrophication monitoring,

795   enabling quantitative assessment of organic matter production and mineralisation (Schneider and Müller, 2018), and can be used as a pivotal parameter to trace acidification (Gustafsson et al., 2023).

800   *Data availability.* The data set will be made available in an openly accessible database upon acceptance.

Author contribution. SL, EJ, GR and UL conceived the study. UL contributed to developing methods and writing the manuscript. GR contributed to developing methods and reviewing the manuscript. EJ contributed by analysing the data and
805 writing and reviewing the manuscript. STS contributed by analysing and visualizing the data and reviewing the manuscript. SL carried out analyses, prepared the figures, and wrote the manuscript with editorial and scientific contributions from all ~~the~~ co-authors.

810 *Competing interests.* The authors declare that they have no conflict of interest.

Acknowledgements. The authors would like to thank Michael Glockzin for his contribution and support with the trace gas measurements, Villu Kikas for his technical assistance, and the crew of the R/V Salme for their help and cooperation. Silvie
815 Lainela´s sincere words of thank you also go to TalTech colleagues Sander Rikka and Ilja Maljutenko for the fruitful discussions in developing and optimising Python and MATLAB scripts and Germo Väli for his help and advice regarding meteorological data. The study was in the frames of the BONUS INTEGRAL project (grant no. 03F0773A), which received funding from BONUS (Art 185), funded jointly by the EU, the German Federal Ministry of Education and Research, the Swedish Research Council Formas, the Academy of Finland, the Polish National Centre for Research and Development, and
820 the Estonian Research Council. The work of Silvie Lainela, Stella-Theresa Stoicescu and Urmas Lips was supported by the Estonian Research Council grant (PRG602). The analysis was also partly supported by the JERICO-S3 project (funded by the European Commission's Horizon 2020 Research and Innovation programme under grant agreements No 871153 and 951799).

825 **References**

Alenius, P., Myrberg, K., and Nekrasov, A.: The physical oceanography of the Gulf of Finland: a review, Boreal Environ. Res., 3, 97-125, 1998.

Alenius, P., Nekrasov, A., and Myrberg, K.: Variability of the baroclinic Rossby radius in the Gulf of Finland, Cont. Shelf Res., 23, 563-573, https://doi.org/10.1016/S0278-4343(03)00004-9, 2003.

830 Andrejev, O., Myrberg, K., Alenius, P., and Lundberg, P.A.: Mean circulation and water exchange in the Gulf of Finland e a study based on three-dimensional modelling, Boreal. Environ. Res., 9, 1-16, 2004.

Astok, V., Otsmann, M., and Suursaar, Ü.: Water exchange as the main physical process in semi-enclosed marine systems: the Gulf of Riga case, Hydrobiologia, 393, 11−18, https://doi.org/10.1023/A:1003517110726, 1999.

Bange, H. W., Bartell, U. H., Rapsomanikis, S., and Andreae, M. O.: Methane in the Baltic and North Seas and a reassessment of the marine emissions of methane, Global Biogeochem. Cy., 8, 465–480, https://doi.org/10.1029/94GB02181, 1994.

Borges, A.V., Champenois, W., Gypens, N., Delille, B. and Harlay, J.: Massive marine methane emissions from near-shore shallow coastal areas, Sci Rep 6, 27908, https://doi.org/10.1038/srep27908, 2016.

Borges, A. V., Speeckaert, G., Champenois, W., Scranton, M. I., and Gypens, N.: Productivity and Temperature as Drivers of Seasonal and Spatial Variations of Dissolved Methane in the Southern Bight of the North Sea, Ecosystems, 21, 583–599, https://doi.org/10.1007/s10021-017-0171-7, 2018.

Canadell, J.G., Monteiro, P.M.S., Costa, M.H., Cotrim da Cunha, L., Cox, P.M., Eliseev, A.V., Henson, S., Ishii, M., Jaccard, S., Koven, C., Lohila, A., Patra, P.K., Piao, S., Rogelj, J., Syampungani, S., Zaehle, S., and Zickfeld, K.: Global Carbon and other Biogeochemical Cycles and Feedbacks, in: Climate Change 2021 - The Physical Science Basis, Contribution of Working Group I to the Sixth Assessment Report of the Intergovernmental Panel on Climate Change, edited by: Masson-Delmotte, V., Zhai, P., Pirani, A., Connors, S.L., Péan, C., Berger, S., Caud, N., Chen, Y., Goldfarb, L., Gomis, M.I., Huang, M., Leitzell, K., Lonnoy, E., Matthews, J.B.R., Maycock, T.K., Waterfield, T., Yelekçi, O., Yu, R., and Zhou, B., Cambridge University Press, 673–816, https://doi.org/10.1017/9781009157896.007, 2023.

Dai, M., Su, J., Zhao, Y., Hofmann, E.E., Cao, Z., Cai, W.-J., Gan, J., Lacroix, F., Laruelle, G.G., Meng, F., Müller, J.D., Regnier, P.A.G., Wang, G., and Wang, Z.: Carbon Fluxes in the Coastal Ocean: Synthesis, Boundary Processes, and Future Trends, Annu. Rev. Earth Pl. Sc., 50, 593-626, https://doi.org/10.1146/annurev-earth-032320-090746, 2022.

De Angelis, M.A. and Lilley, M.D.: Methane in surface waters of Oregon estuaries and rivers, Limnol. Oceanogr., 32, 716-722, https://doi.org/10.4319/lo.1987.32.3.0716, 1987.

Dlugokencky, E. J., Steele, L. P., Lang, P. M., and Masarie, K. A.: The growth rate and distribution of atmospheric methane, J. Geophys. Res., 99, 17021– 17043, https://doi.org/10.1029/94JD01245, 1994.

EMODnet   Geology: https://emodnet.ec.europa.eu/geoviewer/?layers=12494:1:1&basemap=ebwbl&active=12494&bounds=1889347.1962289177,7790646.9624039605,3305342.315828531,8401847.980824888&filters=&projection=EPSG:3857, last access: 25 August 2023.

Friedlingstein, P., O'Sullivan, M., Jones, M. W., Andrew, R. M., Gregor, L., Hauck, J., Le Quéré, C., Luijkx, I. T., Olsen, A., Peters, G. P., Peters, W., Pongratz, J., Schwingshackl, C., Sitch, S., Canadell, J. G., Ciais, P., Jackson, R. B., Alin, S. R., Alkama, R., Arneth, A., Arora, V. K., Bates, N. R., Becker, M., Bellouin, N., Bittig, H. C., Bopp, L., Chevallier, F., Chini, L. P., Cronin, M., Evans, W., Falk, S., Feely, R. A., Gasser, T., Gehlen, M., Gkritzalis, T., Gloege, L., Grassi, G., Gruber, N., Gürses, Ö., Harris, I., Hefner, M., Houghton, R. A., Hurtt, G. C., Iida, Y., Ilyina, T., Jain, A. K., Jersild, A., Kadono, K., Kato, E., Kennedy, D., Klein Goldewijk, K., Knauer, J., Korsbakken, J. I., Landschützer, P., Lefèvre, N., Lindsay, K., Liu, J., Liu, Z., Marland, G., Mayot, N., McGrath, M. J., Metzl, N., Monacci, N. M., Munro, D. R., Nakaoka, S.-I., Niwa, Y., O'Brien, K., Ono, T., Palmer, P. I., Pan, N., Pierrot, D., Pocock, K., Poulter, B., Resplandy, L., Robertson, E., Rödenbeck, C., Rodriguez, C., Rosan, T. M., Schwinger, J., Séférian, R., Shutler, J. D., Skjelvan, I., Steinhoff, T., Sun, Q., Sutton, A. J., Sweeney, C.,

Takao, S., Tanhua, T., Tans, P. P., Tian, X., Tian, H., Tilbrook, B., Tsujino, H., Tubiello, F., van der Werf, G. R., Walker, A. P., Wanninkhof, R., Whitehead, C., Willstrand Wranne, A., Wright, R., Yuan, W., Yue, C., Yue, X., Zaehle, S., Zeng, J., and Zheng, B.: Global Carbon Budget 2022, Earth Syst. Sci. Data, 14, 4811–4900, https://doi.org/10.5194/essd-14-4811-2022, 2022.

Gustafsson, E., Carstensen, J., Fleming, V., Gustafsson, B.G., Hoikkala, L., and Rehder, G.: Causes and consequences of acidification in the Baltic Sea: implications for monitoring and management, Sci. Rep., 13, p.16322, https://doi.org/10.1038/s41598-023-43596-8, 2023.

Gutiérrez-Loza, L., Wallin, M.B., Sahlée, E., Holding, T., Shutler, J.D., Rehder, G., and Rutgersson, A.: Air–sea CO2 exchange in the Baltic Sea—A sensitivity analysis of the gas transfer velocity, J. Mar. Syst., 222, 103603, https://doi.org/10.1016/j.jmarsys.2021.103603, 2021.

Gülzow, W., Rehder, G., Schneider, B., Schneider v. Deimling, J., and Sadkowiak, B.: A new method for continuous measurement of methane and carbon dioxide in surface waters using off-axis integrated cavity output spectroscopy (ICOS): An example from the Baltic Sea, Limnol. Oceanogr. Meth., 9, 176–184, https://doi.org/10.4319/lom.2011.9.176, 2011.

Gülzow, W., Rehder, G., Schneider v. Deimling, J., Seifert, T., and Tóth, Z.: One year of continuous measurements constraining methane emissions from the Baltic Sea to the atmosphere using a ship of opportunity, Biogeosciences, 10, 81–99, https://doi.org/10.5194/bg-10-81-2013, 2013.

Gülzow, W., Gräwe, U., Kedzior, S., Schmale, O., and Rehder, G.: Seasonal variation of methane in the water column of Arkona and Bornholm Basin, western Baltic Sea, J. Marine Syst., 139, 332–347, https://doi.org/10.1016/j.jmarsys.2014.07.013, 2014.

HELCOM: Manual for the Marine Monitoring in the COMBINE Programme of HELCOM, https://helcom.fi/action-areas/monitoring-and-assessment/monitoring-guidelines/combine-manual/ (last access: 16 June 2023), 2017.

HELCOM: HELCOM Thematic assessment of eutrophication 2011-2016. Baltic Sea Environment Proceedings No. 156, Baltic Marine Environment Protection Commission, ISSN 0357-2994, 2018.

Hersbach, H., Bell, B., Berrisford, P., Biavati, G., Horányi, A., Muñoz Sabater, J., Nicolas, J., Peubey, C., Radu, R., Rozum, I., Schepers, D., Simmons, A., Soci, C., Dee, D., and Thépaut, J-N.: ERA5 monthly averaged data on single levels from 1979 to present. Copernicus Clim. Chang. Serv. Clim. Data Store [data set], https://doi.org/10.24381/cds.f17050d7, 2019.

Heyer, J. and Berger, U.: Methane emission from the coastal area in the southern Baltic Sea, Estuar. Coast. Shelf Sc., 51, 13-30, https://doi.org/10.1006/ecss.2000.0616, 2000.

Holding, T., Ashton, I. G., Shutler, J. D., Land, P. E., Nightingale, P. D., Rees, A. P., Brown, I., Piolle, J.-F., Kock, A., Bange, H. W., Woolf, D. K., Goddijn-Murphy, L., Pereira, R., Paul, F., Girard-Ardhuin, F., Chapron, B., Rehder, G., Ardhuin, F., and Donlon, C. J.: The FluxEngine air-sea gas flux toolbox: simplified interface and extensions for in situ analyses and multiple sparingly soluble gases, Ocean Sci., 15, 1707-1728, https://doi.org/10.5194/os-15-1707-2019, 2019.

900 Honkanen, M., Müller, J.D., Seppälä, J., Rehder, G., Kielosto, S., Ylöstalo, P., Mäkelä, T., Hatakka, J., and Laakso, L.: Diurnal cycle of the CO_2 system in the coastal region of the Baltic Sea, Ocean Sci. Discussions, 2020, 1-28, https://doi.org/10.5194/os-2020-115, 2020.

Hoy, A., Hänsel, S., and Maugeri, M.: An endless summer: 2018 heat episodes in Europe in the context of secular temperature variability and change, Int. J. Climatol., 40, 6315-6336, https://doi.org/10.1002/joc.6582, 2020.

905 Humborg, C., Geibel, M. C., Sun, X., McCrackin, M., Mörth, C.-M., Stranne, C., Jakobsson, M., Gustafsson, B., Sokolov, A., Norkko, A., and Norkko, J.: High Emissions of Carbon Dioxide and Methane From the Coastal Baltic Sea at the End of a Summer Heat Wave, Front. Mar. Sci., 6, 493, https://doi.org/10.3389/fmars.2019.00493, 2019.

IOC, SCOR and IAPSO: The International Thermodynamic Equation of Seawater - 2010: Calculation and Use of Thermodynamic Properties, Intergovernmental Oceanographic Commission, Manuals and Guides No. 56. UNESCO (English), 910 196pp., 2010.

Jacobs, E., Bittig, H. C., Gräwe, U., Graves, C. A., Glockzin, M., Müller, J. D., Schneider, B., and Rehder, G.: Upwelling-induced trace gas dynamics in the Baltic Sea inferred from 8 years of autonomous measurements on a ship of opportunity, Biogeosciences, 18, 2679–2709, https://doi.org/10.5194/bg-18-2679-2021, 2021.

Jakobs, G., Rehder, G., Jost, G., Kießlich, K., Labrenz, M., and Schmale, O.: Comparative studies of pelagic microbial methane 915 oxidation within the redox zones of the Gotland Deep and Landsort Deep (central Baltic Sea), Biogeosciences, 10, 7863–7875, https://doi.org/10.5194/bg-10-7863-2013, 2013.

Jakobs, G., Holtermann, P., Berndmeyer, C., Rehder, G., Blumenberg, M., Jost, G., Nausch, G., and Schmale, O.: Seasonal and spatial methane dynamics in the water column of the central Baltic Sea (Gotland Sea), Cont. Shelf Res., 91, 12–25, https://doi.org/10.1016/j.csr.2014.07.005, 2014.

920 Kahru, M., Elken, J., Kotta, I., Simm, M., and Vilbaste, K.: Plankton distributions and processes across a front in the open Baltic sea. Mar. Ecol. Prog. Ser., 20, 101−111, 1984.

Keeling, R. F., Piper, S. C., Bollenbacher, A. F., and Walker, J. S.: Atmospheric Carbon Dioxide Record from Mauna Loa. CDIAC, ESS-DIVE repository [data set], https://doi.org/10.3334/CDIAC/ATG.035, 2009.

Kikas, V. and Lips, U.: Upwelling characteristics in the Gulf of Finland (Baltic Sea) as revealed by Ferrybox measurements 925 in 2007–2013, Ocean Sci., 12, 843–859, https://doi.org/10.5194/os-12-843-2016, 2016.

Knittel, K. and Boetius, A.: Anaerobic oxidation of methane: progress with an unknown process., Annu. Rev. Microbiol., 63, 311–334, https://doi.org/10.1146/annurev.micro.61.080706.093130, 2009.

Kock, A., Gebhardt, S., and Bange, H. W.: Methane emissions from the upwelling area off Mauritania (NW Africa), Biogeosciences, 5, 1119–1125, https://doi.org/10.5194/bg-5-1119-2008, 2008.

930 Kownacka, J., Busch, S., Göbel, J., Gromisz, S., Hällfors, H., Höglander, H., Huseby, S., Jaanus, A., Jakobsen, H. H., Johansen, M., Johansson, M., Jurgensone, I., Liebeke, N., Kobos, J., Kraśniewski, W., Kremp, A., Lehtinen, S., Olenina, I., v.Weber, M., and Wasmund, N.: Cyanobacteria biomass, 1990-2019, HELCOM Balt. Sea Environ. Fact Sheets, Online, Helsinki

Commission, https://helcom.fi/wp-content/uploads/2022/04/BSEFS-Cyanobacteria-biomass-1990-2020.pdf (last access: 16 June 2023), 2022.

935 Kuliński, K. and Pempkowiak, J.: The carbon budget of the Baltic Sea, Biogeosciences, 8, 3219-3230, https://doi.org/10.5194/bg-8-3219-2011, 2011.

Kuliński, K., Schneider, B., Szymczycha, B., and Stokowski, M.: Structure and functioning of the acid–base system in the Baltic Sea, Earth Syst. Dynam., 8, 1107-1120, https://doi.org/10.5194/esd-8-1107-2017, 2017.

Kuss, J., Roeder, W., Wlost, K.-P., and DeGrandpre, M.D.: Time-series of surface water CO_2 and oxygen measurements on a
940 platform in the central Arkona Sea (Baltic Sea): Seasonality of uptake and release, Mar. Chem., 101, 220-232, https://doi.org/10.1016/j.marchem.2006.03.004, 2006.

Laanearu, J. and Lips, U.: Observed thermohaline fields and low-frequency currents in the Narva Bay, Proc Estonian Acad Sci Eng, 9, 91-106, 2003.

Lehtoranta, J., Savchuk, O. P., Elken, J., Kim, D., Kuosa, H., Raateoja, M., Kauppila, P., Räike, A. and Pitkänen, H.:
945 Atmospheric forcing controlling inter-annual nutrient dynamics in the open Gulf of Finland, J. Mar. Syst., 171, 4–20, 2017.

Lepäranta, M. and Myrberg, K.: Physical Oceanography of the Baltic Sea, Springer Science & Business Media, 378 pp., ISBN 3540797033, 2009.

Liblik, T. and Lips, U.: Variability of synoptic-scale quasi-stationary thermohaline stratification patterns in the Gulf of Finland in summer 2009, Ocean Sci., 8, 603–614, https://doi.org/10.5194/os-8-603-2012, 2012.

950 Liblik, T., Laanemets, J., Raudsepp, U., Elken, J., and Suhhova, I.: Estuarine circulation reversals and related rapid changes in winter near-bottom oxygen conditions in the Gulf of Finland, Baltic Sea, Ocean Sci., 9, 917-930, https://doi.org/10.5194/os-9-917-2013, 2013.

Liblik, T., Väli, G., Salm, K., Laanemets, J., Lilover, M.-J., and Lips, U.: Quasi-steady circulation regimes in the Baltic Sea, Ocean Sci., 18, 857–879, https://doi.org/10.5194/os-18-857-2022, 2022.

955 Lilover, M.J., Lips, U., Laanearu, J. and Liljebladh, B.: Flow regime in the Irbe Strait, Aquat. Sci., 60, 253-265, 1998.

Lips, I. and Lips, U.: Abiotic factors influencing cyanobacterial bloom development in the Gulf of Finland (Baltic Sea), Hydrobiologia, 614, 133-140, https://doi.org/10.1007/s10750-008-9449-2, 2008.

Lips, I., Lips, U., and Liblik, T.: Consequences of coastal upwelling events on physical and chemical patterns in the central Gulf of Finland (Baltic Sea), Cont. Shelf Res., 29, 1836–1847, https://doi.org/10.1016/j.csr.2009.06.010, 2009.

960 Lips, I., Rünk, N., Kikas, V., Meerits, A., and Lips, U.: High-resolution dynamics of the spring bloom in the Gulf of Finland of the Baltic Sea, J. Mar. Syst., 129, 135-149, https://doi.org/10.1016/j.jmarsys.2013.06.002, 2014.

Lips, U., Kikas, V., Liblik, T., and Lips, I.: Multi-sensor in situ observations to resolve the sub-mesoscale features in the stratified Gulf of Finland, Baltic Sea, Ocean Sci., 12, 715−732, https://doi.org/10.5194/os-12-715-2016, 2016a.

Lips, U., Zhurbas, V., Skudra, M., and Väli, G.: A numerical study of circulation in the Gulf of Riga, Baltic Sea. Part I: Whole-
965 basin gyres and mean currents, Cont. Shelf Res., 112, 1-13, https://doi.org/10.1016/j.csr.2015.11.008, 2016b.

Lips, U., Laanemets, J., Lips, I., Liblik, T., Suhhova, I., and Suursaar, Ü.: Wind-driven residual circulation and related oxygen and nutrient dynamics in the Gulf of Finland (Baltic Sea) in winter, Estuar. Coast. Shelf S., 195, 4−15, https://doi.org/10.1016/j.ecss.2016.10.006, 2017.

970 Maljutenko, I. and Raudsepp, U.: Long-term mean, interannual and seasonal circulation in the Gulf of Finland — The wide salt wedge estuary or gulf type ROFI, J. Mar. Syst., 195, 1−19. https://doi.org/10.1016/j.jmarsys.2019.03.004, 2019.

Müller, J. D., Schneider, B., and Rehder, G.: Long-term alkalinity trends in the Baltic Sea and their implications for CO2-induced acidification, Limnol. Oceanogr., 61, 1984–2002, https://doi.org/10.1002/lno.10349, 2016.

Müller, J.D., Schneider, B., Gräwe, U., Fietzek, P., Wallin, M.B., Rutgersson, A., Wasmund, N., Krüger, S. and Rehder, G.: Cyanobacteria net community production in the Baltic Sea as inferred from profiling pCO2 measurements, Biogeosciences, 18,

975 4889-4917, https://doi.org/10.5194/bg-18-4889-2021, 2021.

Myllykangas, J.P., Hietanen, S., and Jilbert, T.: Legacy effects of eutrophication on modern methane dynamics in a boreal estuary, Estuaries Coasts, 43, 189-206, https://doi.org/10.1007/s12237-019-00677-0, 2020.

Myrberg, K. and Andrejev, O.: Main upwelling regions in the Baltic Sea-a statistical analysis based on three-dimensional modelling, Boreal Environ. Res., 8, 97-112, 2003.

980 Nightingale, P.D., Malin, G., Law, C.S., Watson, A.J., Liss, P.S., Liddicoat, M.I., Boutin, J., and Upstill-Goddard, R.C.: In situ evaluation of air-sea gas exchange parameterizations using novel conservative and volatile tracers, Global Biogeochem. Cy., 14, 373-387, https://doi.org/10.1029/1999GB900091, 2000.

Norman, M., Parampil, S. R., Rutgersson, A., and Sahlée, E.: Influence of coastal upwelling on the air–sea gas exchange of CO2 in a Baltic Sea Basin, Tellus B, 65, 21 831, https://doi.org/10.3402/tellusb.v65i0.21831, 2013.

985 Ojaveer, E. (Ed.): Ecosystem of the Gulf of Riga between 1920 and 1990, Estonian Academy Publishers, Tallinn, 1995.

Otsmann, M., Suursaar, Ü., and Kullas, T.: The oscillatory nature of the flows in the system of straits and small semienclosed basins of the Baltic Sea, Cont. Shelf Res., 21, 1577−1603, https://doi.org/10.1016/S0278-4343(01)00002-4, 2001.

Parard, G., Rutgersson, A., Raj Parampil, S., and Charantonis, A. A.: The potential of using remote sensing data to estimate air–sea CO₂ exchange in the Baltic Sea, Earth Syst. Dynam., 8, 1093–1106, https://doi.org/10.5194/esd-8-1093-2017, 2017.

990 Pavelson, J.: Mesoscale physical processes and the related impact on the summer nutrient fields and phytoplankton blooms in the western Gulf of Finland, Ph.D. thesis, Department of Marine Systems, Tallinn University of Technology, Estonia, 38 pp., 2005.

Placke, M., Meier, H. E. M., Gräwe, U., Neumann, T., Frauen, C., and Liu, Y.: Long-Term Mean Circulation of the Baltic Sea as Represented by Various Ocean Circulation Models, Front. Mar. Sci., 5, 287, https://doi.org/10.3389/fmars.2018.00287,

995 2018.

Richey, J.E., Devol, A.H., Wofsy, S.C., Victoria, R., and Riberio, M.N.: Biogenic gases and the oxidation and reduction of carbon in Amazon River and floodplain waters, Limnol. Oceanogr., 33, 551-561, https://doi.org/10.4319/lo.1988.33.4.0551, 1988.

Reeburgh, W.S.: Oceanic methane biogeochemistry, Chem. Rev., 107, 486–513, https://doi.org/10.1021/cr050362v, 2007.

1000   Roth, F., Sun, X., Geibel, M.C., Prytherch, J., Brüchert, V., Bonaglia, S., Broman, E., Nascimento, F., Norkko, A., and Humborg, C.: High spatiotemporal variability of methane concentrations challenges estimates of emissions across vegetated coastal ecosystems, Global Change Biol., 28, 4308–4322, https://doi.org/10.1111/gcb.16177, 2022.

Rutgersson, A., Smedman, A., and Sahlée, E.: Oceanic convective mixing and the impact on air-sea gas transfer velocity, Geophys. Res. Lett., 38, https://doi.org/10.1029/2010GL045581, 2011.

1005   Sabbaghzadeh, B., Arévalo-Martínez, D.L., Glockzin, M., Otto, S., and Rehder, G.: Meridional and Cross-Shelf Variability of N2O and CH4 in the Eastern-South Atlantic, J. Geophys. Res.-Oceans, 126, e2020JC016878, https://doi.org/10.1029/2020JC016878, 2021.

Schlitzer, R.: Ocean Data View [code], https://odv.awi.de, last access: 29 November 2022.

Schmale, O., Schneider v. Deimling, J., Gülzow, W., Nausch, G., Waniek, J. J., and Rehder, G.: Distribution of methane in
1010   the water column of the Baltic Sea, Geophys. Res. Lett., 37, L12 604, https://doi.org/10.1029/2010GL043115, 2010.

Schmale, O., Wäge, J., Mohrholz, V., Wasmund, N., Gräwe, U., Rehder, G., Labrenz, M., and Loick-Wilde, N.: The contribution of zooplankton to methane supersaturation in the oxygenated upper waters of the central Baltic Sea, Limnol. Oceanogr., 63, 412–430, https://doi.org/10.1002/lno.10640, 2018.

Schneider, B., Gülzow, W., Sadkowiak, B., and Rehder, G.: Detecting sinks and sources of CO2 and CH4 by ferrybox-based
1015   measurements in the Baltic Sea: Three case studies, J. Mar. Syst., 140, 13-25, https://doi.org/10.1016/j.jmarsys.2014.03.014, 2014.

Schneider, B. and Müller, J. D.: Biogeochemical Transformations in the Baltic Sea, Springer Oceanography, Springer International Publishing, Cham, Switzerland, https://doi.org/10.1007/978-3-319-61699-5, 2018.

Seppälä, J. and Balode, M.: Spatial distribution of phytoplankton in the Gulf of Riga during spring and summer stages, J. Mar.
1020   Syst., 23, 51-67, https://doi.org/10.1016/S0924-7963(99)00050-0, 1999.

Shutler JD, Land PE, Piolle JF, Woolf DK, Goddijn-Murphy L, Paul F, Girard-Ardhuin F, Chapron B., and Donlon CJ.: FluxEngine: a flexible processing system for calculating atmosphere-ocean carbon dioxide gas fluxes and climatologies, J. Atmos. Ocean. Tech., 33, 741-756, https://doi.org/10.1175/JTECH-D-14-00204.1, 2016.

Skudra, M. and Lips, U.: Characteristics and inter-annual changes in temperature, salinity and density distribution in the Gulf
1025   of Riga, Oceanologia, 59, 37-48, https://doi.org/10.1016/j.oceano.2016.07.001, 2017.

Soosaar, E., Maljutenko, I., Uiboupin, R., Skudra, M., and Raudsepp, U.: River bulge evolution and dynamics in a non-tidal sea – Daugava River plume in the Gulf of Riga, Baltic Sea, Ocean Sci., 12, 417−432, https://doi.org/10.5194/os-12-417-2016, 2016.

Stawiarski, B., Otto, S., Thiel, V., Gräwe, U., Loick-Wilde, N., Wittenborn, A. K., Schloemer, S., Wäge, J., Rehder, G.,
1030   Labrenz, M., Wasmund, N., and Schmale, O.: Controls on zooplankton methane production in the central Baltic Sea, Biogeosciences, 16, 1−16, https://doi.org/10.5194/bg-16-1-2019, 2019.

Stålnacke, P., Grimvall A., Sundblad K., and Tonderski A.: Estimation of riverine loads of nitrogen and phosphorus to the Baltic Sea, 1970–1993, Environ. Monit. Assess., 58, 173−200, https://doi.org/10.1023/A:1006073015871, 1999.

Stiebrins, O. and Väling, P.: Bottom sediments of the Gulf of Riga, Geol. Surv. Latv. Riga, 4, ISBN 9984-9130-0-7, 1996.

1035   Stoicescu, S.-T., Lips, U., and Liblik, T.: Assessment of Eutrophication Status Based on Sub-Surface Oxygen Conditions in the Gulf of Finland (Baltic Sea), Front. Mar. Sci., 6, 54, https://doi.org/10.3389/fmars.2019.00054, 2019.

Stoicescu, S.-T., Laanemets, J., Liblik, T., Skudra, M., Samlas, O., Lips, I., and Lips, U.: Causes of the extensive hypoxia in the Gulf of Riga in 2018, Biogeosciences, 19, 2903–2920, https://doi.org/10.5194/bg-19-2903-2022, 2022.

Suursaar, Ü., Kullas, T., and Otsmann M.: The influence of currents and waves on ecological conditions of the Väinameri.
1040   Proc. Estonian Acad. Sci. Biol. Ecol., 50, 231-247, 2001.

Takahashi, T., Olafsson, J., Goddard, J. G., Chipman, D.W., and Sutherland, S. C.: Seasonal variation of CO2 and nutrients in the high-latitude surface oceans: A comparative study, Global Biogeochem. Cy., 7, 843–878, https://doi.org/10.1029/93GB02263, 1993.

Thomas, H. and Schneider, B.: The seasonal cycle of carbon dioxide in Baltic Sea surface waters, J. Mar. Syst., 22, 53-67,
1045   https://doi.org/10.1016/S0924-7963(99)00030-5, 1999.

Townsend, D.W., Cammen, L.M., Holligan, P.M., Campbell, D., and Pettigrew, N.R.: Causes and consequences of variability in the timing of spring phytoplankton blooms, Deep-Sea Res. Pt. I, 41, 747–765, https://doi.org/10.1016/0967-0637(94)90075-2, 1994.

Valentine, D.L.: Biogeochemistry and microbial ecology of methane oxidation in anoxic environments: a review, A. Van
1050   Leeuw., 81, 271-282, https://doi.org/10.1023/A:1020587206351, 2002.

Wanninkhof, R.: Relationship between wind speed and gas exchange over the ocean revisited, Limnol. Oceanogr. Meth., 12, 351–362, https://doi.org/10.4319/lom.2014.12.351, 2014.

Weber, T., Wiseman, N. A., and Kock, A.: Global ocean methane emissions dominated by shallow coastal waters, Nat. Commun., 10, 4584, https://doi.org/10.1038/s41467-019-12541-7, 2019.

1055   Weiss, R. F. and Price, B. A.: Nitrous oxide solubility in water and seawater, Mar. Chem., 8, 347–359, https://doi.org/10.1016/0304-4203(80)90024-9, 1980.

Wesslander, K., Omstedt, A., and Schneider, B.: Inter-annual and seasonal variations in the air–sea CO2 balance in the central Baltic Sea and the Kattegat, Cont. Shelf Res., 30, 1511-1521, https://doi.org/10.1016/j.csr.2010.05.014, 2010.

Wesslander, K., Hall, P., Hjalmarsson, S., Lefevre, D., Omstedt, A., Rutgersson, A., Sahlée, E., and Tengberg, A.: Observed
1060   carbon dioxide and oxygen dynamics in a Baltic Sea coastal region, J. Mar. Syst., 86, 1-9, https://doi.org/10.1016/j.jmarsys.2011.01.001, 2011

Wiesenburg, D. A. and Guinasso, N. L.: Equilibrium solubilities of methane, carbon monoxide, and hydrogen in water and sea water, J. Chem. Eng. Data, 24, 356–360, https://doi.org/10.1021/je60083a006, 1979.

Woolf, D.K., Land, P.E., Shutler, J.D., Goddijn-Murphy, L.M., and Donlon, C.J.: On the calculation of air-sea fluxes of CO2
1065   in the presence of temperature and salinity gradients, J. Geophys. Res.-Oceans, 121, 1229-1248, https://doi.org/10.1002/2015JC011427, 2016.

Yurkovskis, A., Wulff, F., Rahm, L., Andruzaitis, A., and Rodriguez-Medina, M.: A Nutrient Budget of the Gulf of Riga; Baltic Sea, Estuar. Coast. Shelf S., 37, 113–127, https://doi.org/10.1006/ecss.1993.1046, 1993.